CHAPTER

4

Microwave Dielectric Properties of Natural Earth Materials

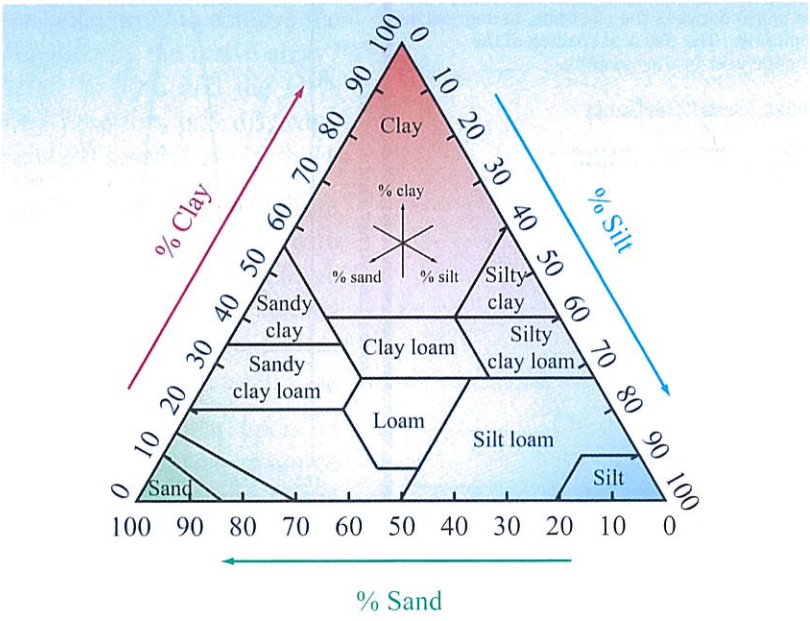

Soil textural triangle

CONTENTS

Overview

4-1 Pure-water single-Debye dielectric model ($f \leq 50$ GHz)

4-2 Saline-water double-Debye dielectric model ($f \leq 1000$ GHz)

4-3 Dielectric constant of pure ice

4-4 Dielectric mixing models for heterogeneous materials

4-5 Sea ice

4-6 Dielectric constant of snow

4-7 Dielectric constant of dry rocks

4-8 Dielectric constant of soils

4-9 Dielectric constant of vegetation

Overview

This chapter is a sourcebook of representative models and measured data of the microwave dielectric properties of natural earth materials. These materials can generally be classified into one of the following dielectric groups: (a) ***homogeneous substances***, (b) ***electrolytic solutions***, or (c) ***heterogeneous mixtures***. Only pure water and ice belong to group (a). Ionic salts or sugars dissolved in water produce an electrolytic solution whose microwave dielectric properties may be markedly different from those of pure water. Section 4-2 therefore examines the dielectric properties of both pure and saline water, and Section 4-3 treats the case for pure ice.

Heterogeneous mixtures include: sea ice (a mixture of ice crystals, air pockets, and liquid brine inclusions); snow (a mixture of air, ice particles, and sometimes liquid water inclusions); dry soil (a mixture of soil particles and air); wet soil; vegetation; and other materials. For a medium consisting of a ***host material*** with an intrinsic relative dielectric constant ε_h, within which is contained a homogeneous random concentration of ellipsoidal particles (***inclusions***) of material with an intrinsic relative dielectric constant ε_i, the relative dielectric constant of the ***mixture***, ε_m, is said to consist of two components,

$$\varepsilon_m(x,y,z;\hat{\mathbf{p}}) = \varepsilon_m(\hat{\mathbf{p}}) + \varepsilon_f(x,y,z;\hat{\mathbf{p}}), \tag{4.1}$$

where $\varepsilon_m(\hat{\mathbf{p}}) = \langle \varepsilon_m(x,y,z;\hat{\mathbf{p}}) \rangle$ is the ***effective or average*** value of the dielectric constant of the medium and ε_f is the ***fluctuating component***. Thus, $\varepsilon_m(\hat{\mathbf{p}})$ is independent of position within the medium but may be a function of the polarization unit vector $\hat{\mathbf{p}}$, which denotes the direction of the electric field of the incident wave relative to the geometry of the ellipsoids if the ellipsoids have a preferred orientation. If the orientation is random, ε_m becomes independent of the direction of the incident field. The fluctuating component ε_f accounts for the deviation from the average value $\varepsilon_m(\hat{\mathbf{p}})$ at any point (x,y,z) within the medium. Its average value $\langle \varepsilon_f \rangle = 0$.

The propagation constant of the medium, γ, is governed by the average dielectric constant $\varepsilon_m(\hat{\mathbf{p}})$, as discussed below. The significance of the fluctuating component ε_f, or rather of its statistical spatial distribution, has to do with volume scattering in the medium. Volume scattering is treated in Chapter 11 and therefore is not addressed in this chapter. Instead, we focus our attention on methods of relating the average dielectric constant ε_m of the mixture to the dielectric properties and volume fractions of the constituents. A brief review of dielectric mixing models is given in Section 4-4, followed in succeeding sections by a survey of measured dielectric constant data and applicable models for several heterogeneous mixtures of interest, including sea ice, snow, rocks and powders, soils, and vegetation. Microwave dielectric measurement techniques are not covered in this chapter; the interested reader is referred to Bussey (1967), Nicolson and Ross (1970), Weir (1974), Jones (1976), Campbell (1978), Stuchly and Stuchly (1980), Hallikainen et al. (1986), and El-Rayes and Ulaby (1987).

Throughout this book, the symbol ε refers to the ***average relative dielectric constant of the material*** under consideration, and its first subscript denotes the name of the material (except for ε_0, the permittivity of free space). In general, ε is complex, consisting of a real part, ε', and an imaginary part, ε'',

$$\varepsilon = \varepsilon' - j\varepsilon'', \tag{4.2}$$

where ε' is the ***relative permittivity*** of the material and ε'' is its ***dielectric loss factor***.

The dielectric constant ε is related to the complex ***index of refraction*** n through

$$\varepsilon = n^2. \tag{4.3}$$

With n defined as

$$n = n' - jn'', \tag{4.4}$$

it follows that

$$\varepsilon' = (n')^2 - (n'')^2, \qquad \varepsilon'' = 2n'n'', \tag{4.5}$$

and, conversely,

$$n' = \mathfrak{Re}\left\{\sqrt{\varepsilon}\right\}, \qquad n'' = -\mathfrak{Im}\left\{\sqrt{\varepsilon}\right\}. \tag{4.6}$$

For a plane wave propagating in a lossy medium in the z direction, the electric-field intensity at a distance z is given by

$$E(z) = E_0 \exp(-\gamma z), \tag{4.7}$$

where E_0 is the field intensity at $z = 0$ and

$$\gamma = \alpha + j\beta, \tag{4.8}$$

where γ, α, and β are the ***propagation***, ***absorption***, and ***phase*** constants of the medium. They are related to n and ε by

$$\alpha = k_0 n'' = -k_0 \, \Im\mathrm{m}\left\{\sqrt{\varepsilon}\right\} \quad \text{Np/m}, \tag{4.9a}$$

$$\beta = k_0 n' = k_0 \, \Re\mathrm{e}\left\{\sqrt{\varepsilon}\right\} \quad \text{rad/m}, \tag{4.9b}$$

where $k_0 = 2\pi/\lambda_0$ is the wave number in free space, and λ_0 is the free-space wavelength in meters.

Ignoring scattering losses in the medium, the power density $\mathcal{S}(z)$ at a point z is given by

$$\mathcal{S}(z) = \mathcal{S}_0 \exp(-\kappa_a z), \tag{4.10}$$

where κ_a, the ***power absorption coefficient***, is related to α by

$$\kappa_a = 2\alpha. \tag{4.11}$$

A related quantity of interest in remote sensing is the ***penetration depth*** δ_p. For a scatter-free medium,

$$\delta_p = 1/\kappa_a \qquad \text{(m)}, \tag{4.12a}$$

and if $\varepsilon''/\varepsilon' \ll 1$,

$$\delta_p \approx \frac{\sqrt{\varepsilon'}}{k_0 \varepsilon''}. \tag{4.12b}$$

Note that δ_p is related to the ***skin depth*** δ_s by $\delta_p = \delta_s/2$.

4-1 Pure-Water Single-Debye Dielectric Model ($f \leq 50$ GHz)

For pure (distilled) water with no dissolved salts, we offer two dielectric models, a relatively simple model applicable to frequencies $f \leq 50$ GHz, and a more elaborate model applicable to frequencies as high as 1000 GHz. The latter is a special case of the saline water model of Section 4-2.

Until the mid-1990s, the general consensus within the microwave community was that the dielectric constant of water obeys the single-relaxation Debye model for polar molecules (Hasted, 1973), namely

$$\varepsilon_w = \varepsilon_{w\infty} + \frac{\varepsilon_{w0} - \varepsilon_{w\infty}}{1 + j2\pi f \tau_w}, \tag{4.13}$$

where

ε_{w0} = static dielectric constant (at $f = 0$), dimensionless,
$\varepsilon_{w\infty}$ = high-frequency dielectric constant (as $f \to \infty$), dimensionless,
τ_w = relaxation time constant (s)
f = frequency (Hz).

Rationalizing Eq. (4.13) and equating it to $\varepsilon_w = \varepsilon_w' - j\varepsilon_w''$ leads to

$$\varepsilon_w' = \varepsilon_{w\infty} + \frac{\varepsilon_{w0} - \varepsilon_{w\infty}}{1 + (2\pi f \tau_w)^2}, \tag{4.14a}$$

$$\varepsilon_w'' = \frac{2\pi f \tau_w (\varepsilon_{w0} - \varepsilon_{w\infty})}{1 + (2\pi f \tau_w)^2}. \tag{4.14b}$$

In addition to their dependence on frequency, ε_w' and ε_w'' also are temperature-dependent because ε_{w0}, τ_w, and (possibly) $\varepsilon_{w\infty}$ are all functions of the water temperature T.

The magnitude of the high-frequency dielectric constant $\varepsilon_{w\infty}$ was determined by Lane and Saxton (1952) to be

$$\varepsilon_{w\infty} = 4.9. \tag{4.15}$$

Contradictory views have been expressed on the temperature dependence of $\varepsilon_{w\infty}$; but the dependence is so weak that for computational purposes $\varepsilon_{w\infty}$ may be considered a constant equal to 4.9.

The relaxation time of pure water is given by

$$2\pi\tau_w(T) = 1.1109 \times 10^{-10} - 3.824 \times 10^{-12} T + 6.938 \times 10^{-14} T^2 - 5.096 \times 10^{-16} T^3, \tag{4.16}$$

where T is in °C. This expression was obtained by Stogryn (1971) by fitting a polynomial to experimental data. A related term used in the literature is the ***relaxation frequency*** f_0, where

$$f_0 = (2\pi\tau_w)^{-1}. \tag{4.17}$$

The relaxation frequency of pure water lies in the microwave region; f_0 (0 °C) $\approx$ 8.9 GHz and f_0 (20 °C) $\approx$ 16.7 GHz. From Eq. (4.14), it can be shown that ε''_w has its maximum value at $f = f_0$.

Using dielectric measurements made at 1.43 GHz and 2.65 GHz, Klein and Swift (1977) generated the following regression fit for $\varepsilon_{w0}(T)$:

$$\varepsilon_{w0}(T) = 88.045 - 0.4147T + 6.295 \times 10^{-4}T^2 + 1.075 \times 10^{-5}T^3. \tag{4.18}$$

We shall refer to the group of expressions given by Eqs. (4.14) through (4.18) as the ***single-Debye dielectric model*** (or SD^{2}M) for pure water.

The plots in Fig. 4-1 depict the frequency responses of ε'_w and ε''_w of pure water at $T = 0$ °C and 20 °C. They cover the frequency range from 0 to 50 GHz. We observe that the two sets of spectral plots have the same general shape, but their absolute levels are different at the two different temperatures, and the relaxation frequency (frequency at which ε''_w is a maximum) shifts from 8.9 GHz at 0 °C to 16.7 GHz at 20 °C.

Values computed using SD^{2}M are found to be in excellent agreement with experimental measurements conducted at frequencies below 50 GHz across the temperature range $0 \leq T \leq 30$ °C. The error is less than 5%, and at frequencies below 10 GHz it is within 1%.

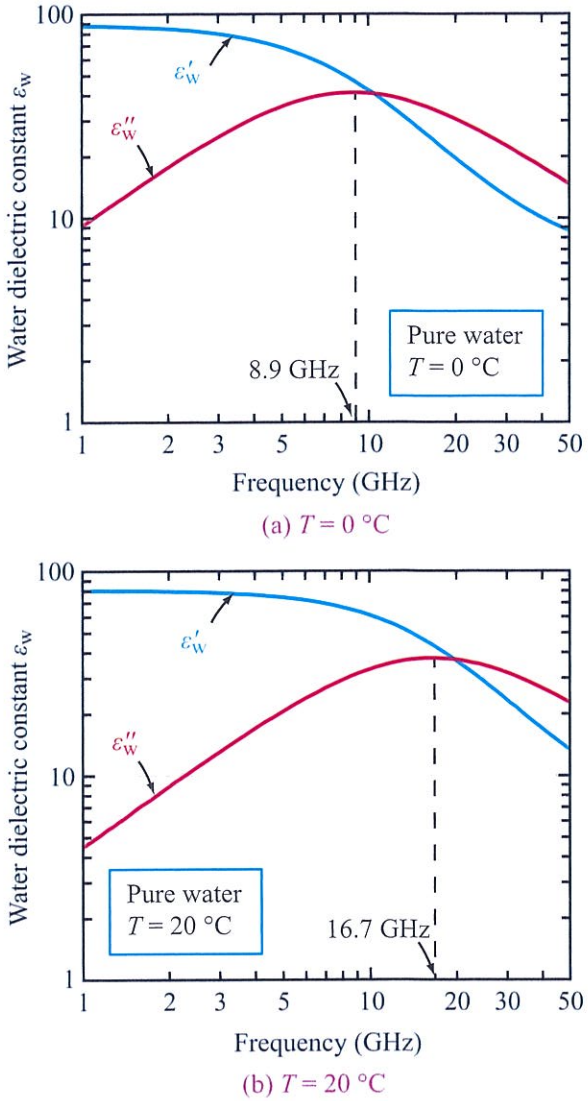

Figure 4-1: Microwave spectra of the permittivity and dielectric loss factor of pure water at (a) 0 °C and (b) 20 °C.

4-2 Saline-Water Double-Debye Dielectric Model ($f \leq 1000$ GHz)

[†]A review of the literature suggests that the most accurate model available at the present time for computing the dielectric constant of water is based on a ***double-Debye dielectric model*** (D3M) developed by William Ellison and reported in the book edited by Mätzler (2006, pp. 431–455). The D3M, which was developed for seawater (and reduces to a model for pure water when the water salinity is set to zero) is given by

$$\varepsilon'_w = \varepsilon_{w\infty} + \frac{\varepsilon_{w0} - \varepsilon_{w1}}{1 + (2\pi f\tau_{w1})^2} + \frac{\varepsilon_{w0} - \varepsilon_{w\infty}}{1 + (2\pi f\tau_{w2})^2}, \tag{4.19a}$$

[†]**Computer Code 4.1 (pure water); Computer Code 4.2 (saline water).**

$$\varepsilon''_w = \frac{2\pi f\tau_{w1}(\varepsilon_{w0}-\varepsilon_{w1})}{1+(2\pi f\tau_{w1})^2} + \frac{2\pi f\tau_{w2}(\varepsilon_{w0}-\varepsilon_{w\infty})}{1+(2\pi f\tau_{w2})^2} + \frac{\sigma_i}{2\pi\varepsilon_0 f}, \quad (4.19b)$$

where ε_0 is the permittivity of free space. The expression given by Eq. (4.19a) contains two relaxation terms, one with a relaxation time constant τ_{w1} and another with τ_{w2}. The same is true for ε''_w, which implies that the spectral plot of ε''_w should exhibit maxima at two relaxation frequencies,

$$f_{01} = \frac{1}{2\pi\tau_{w1}}, \qquad f_{02} = \frac{1}{2\pi\tau_{w2}}. \quad (4.20)$$

At $T = 0$ °C, $f_{01} = 8.9$ GHz and $f_{02} = 201.8$ GHz. The expression for ε''_w also includes a term proportional to the ionic conductivity σ_i of the water solution when the solution contains dissolved salts. For pure water, $\sigma_i = 0$.

As noted earlier in Section 4-1, the dielectric spectrum of water exhibits a relaxation frequency in the microwave region ($f_0 = 8.9$ GHz at 0 °C). The suggestion to add a second relaxation frequency was first made in the 1950s, but it was not seriously considered until several new experimental measurements were conducted in the mid-1990s (Barthel et al., 1990; Kindt et al., 1996; Stogryn et al., 1996; Rønne et al., 1997). Using the double-Debye model and all available, credible dielectric data for pure and saline water, Ellison (in Mätzler, 2006, pp. 431–455) generated empirical functions for all of the parameters in Eq. (4.19). The applicable range of conditions is:

$$0 \le T \le 30°\text{C},$$
$$0 \le S \le 40‰ \text{ or } 40 \text{ psu},$$
$$0 \le f \le 1000 \text{ GHz},$$

where S is the water ***salinity***, defined as the total mass of solid salt in grams dissolved in one kilogram of solution. Thus, S is in parts per thousand (‰) on a weight basis. Instead of using the symbol (‰), salinity has been given the equivalent unit of psu, which stands for ***practical salinity unit***, with 1 psu = 1 (‰). For pure water, $S = 0$.

The parameter functions are:

$$\varepsilon_{w0} = 87.85306 \cdot \exp\{-0.00456992T - a_1S - a_2S^2 - a_3ST\}, \quad (4.21a)$$

$$\varepsilon_{w1} = a_4 \exp\{-a_5T - a_6S - a_7ST\}, \quad (4.21b)$$

$$\tau_{w1} = (a_8 + a_9S)\exp\left(\frac{a_{10}}{T+a_{11}}\right) \text{ ns}, \quad (4.21c)$$

$$\tau_{w2} = (a_{12} + a_{13}S)\exp\left(\frac{a_{14}}{T+a_{15}}\right) \text{ ns}, \quad (4.21d)$$

$$\varepsilon_{w\infty} = a_{16} + a_{17}T + a_{18}S, \quad (4.21e)$$

$$\sigma_i = \sigma(T,35)\cdot P(S)\cdot Q(T,S), \quad (4.21f)$$

where

$$\sigma(T,35) = 2.903602 + 8.607\cdot 10^{-2}T + 4.738817\cdot 10^{-4}T^2 - 2.991\cdot 10^{-6}T^3 + 4.3041\cdot 10^{-9}T^4, \quad (4.21g)$$

$$P(S) = S\,\frac{37.5109 + 5.45216S + 0.014409S^2}{1004.75 + 182.283S + S^2}, \quad (4.21h)$$

$$Q(T,S) = 1 + \frac{\alpha_0(T-15)}{T+\alpha_1}, \quad (4.21i)$$

$$\alpha_0 = \frac{6.9431 + 3.2841S - 0.099486S^2}{84.85 + 69.024S + S^2}, \quad (4.21j)$$

$$\alpha_1 = 49.843 - 0.2276S + 0.00198S^2. \quad (4.21k)$$

Coefficients a_1 to a_{18} are listed in Table 4-1. According to Ellison (in Mätzler, 2006, p. 454), this semiempirical model represents the dielectric constant "of pure water to within 1% over the frequency range 0–20 GHz, to within 3% over 30–100 GHz, and to within 5% over 100–1000 GHz." He also adds that for seawater, the model is accurate to within 3% (of experimental data) over the frequency range 3–105 GHz. As there are no reported experimental measurements of the dielectric constant of seawater at frequencies greater than 105 GHz, it is not possible to ascertain the accuracy of the model at $f > 105$ GHz.

Figures 4-2(a) and 4-2(b) display the frequency responses of ε'_w and ε''_w for pure water and seawater

Table 4-1: Values of coefficients in Eq. (4.21) of D3M (Double-Debye dielectric model) [Mätzler, 2006].

$a_1 = 0.46606917\text{E}-02$
$a_2 = -0.26087876\text{E}-04$
$a_3 = -0.63926782\text{E}-05$
$a_4 = 0.63000075\text{E}+01$
$a_5 = 0.26242021\text{E}-02$
$a_6 = -0.42984155\text{E}-02$
$a_7 = 0.34414691\text{E}-04$
$a_8 = 0.17667420\text{E}-03$
$a_9 = -0.20491560\text{E}-06$
$a_{10} = 0.58366888\text{E}+03$
$a_{11} = 0.12684992\text{E}+03$
$a_{12} = 0.69227972\text{E}-04$
$a_{13} = 0.38957681\text{E}-06$
$a_{14} = 0.30742330\text{E}+03$
$a_{15} = 0.12634992\text{E}+03$
$a_{16} = 0.37245044\text{E}+01$
$a_{17} = 0.92609781\text{E}-02$
$a_{18} = -0.26093754\text{E}-01$

at 20 °C, calculated using the D3M expressions in Eqs. (4.19) and (4.21). The average salinity of seawater is $S = 32.54$ psu. Whereas the relaxation phenomenon at $f_{01} = 16.7$ GHz is clearly visible in the plots of Fig. 4-2, the effect is much more subtle at $f_{02} = 281.4$ GHz. Moreover, ε'_{w} of pure water and ε'_{sw} of seawater are approximately the same over the entire spectrum from 1 to 1000 GHz, and so are the loss factors ε''_{w} and ε''_{w} at frequencies above the relaxation frequency f_{01}, but $\varepsilon''_{\text{sw}}$ of seawater is much larger than ε''_{w} of pure water at frequencies below f_{01}.

For the sake of completeness, the reader is referred to another equally credible model developed by Meissner and Wentz (2004). The model uses the same double-Debye expressions given by Eq. (4.19) and relies on basically the same experimental data used by Ellison (Mätzler, 2006), but the forms of the parameter functions are different from those developed by Ellison.

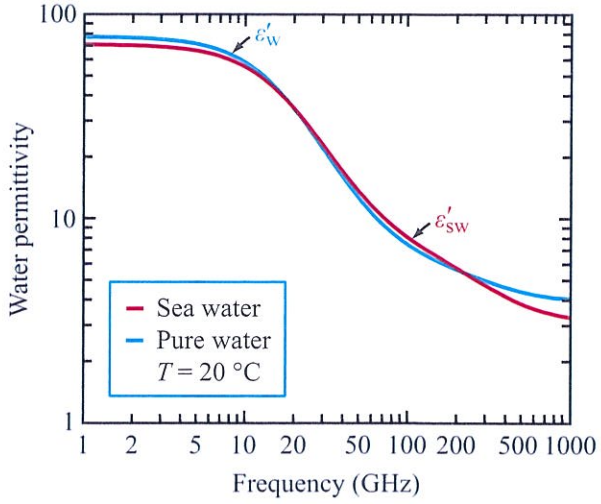

(a) Permittivity

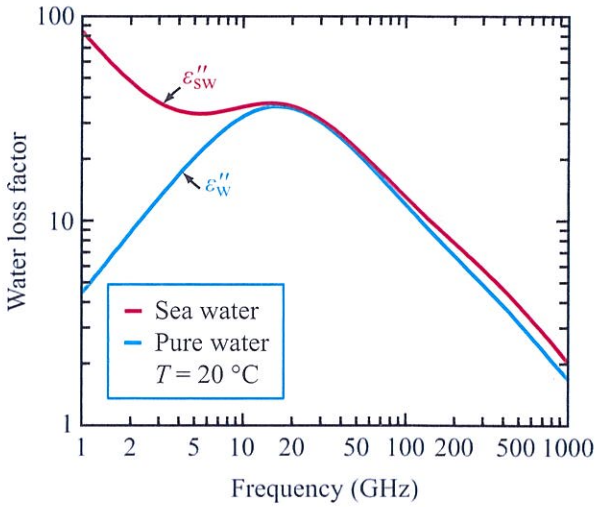

(b) Loss factor

Figure 4-2: Microwave spectra of (a) the permittivities and (b) loss factors of pure water (ε_{w}) and seawater (ε_{sw}) at $T = 20$ °C. Sea salinity is 32.54 psu.

4-3 Dielectric Constant of Pure Ice

Unlike liquid water, whose relaxation frequencies lie in the microwave region, the relaxation frequency of pure ice f_{i0} occurs in the kilohertz region. Hence, in the microwave region (where f is on the order of 10^9 Hz),

the quantity

$$2\pi f\tau_i = \frac{f}{f_{i0}} \gg 1.$$

Consequently, for ice the Debye model expressions of the form given by Eq. (4.14) simplify to

$$\varepsilon_i' \approx \varepsilon_{i\infty}, \tag{4.22a}$$

$$\varepsilon_i'' \approx \frac{\varepsilon_{i0} - \varepsilon_{i\infty}}{2\pi f\tau_i} = \frac{\alpha_0}{f}, \tag{4.22b}$$

where $\alpha_0 = (\varepsilon_{i0} - \varepsilon_{i\infty})/2\pi\tau_i$. According to Mätzler and Wegmüller (1987), ε_i' is essentially independent of frequency from 10 MHz to 300 GHz, and it exhibits a weak temperature dependence of the form:

$$\varepsilon_i' = 3.1884 + 9.1\times 10^{-4}T \quad (-40^\circ\text{C} \le T \le 0), \tag{4.23}$$

where T is the temperature in °C. In practice, we can ignore the temperature dependence and use $\varepsilon_i' \approx 3.2$ across the entire microwave spectrum.

In Eq. (4.22b), ε_i'' varies as $1/f$ and the coefficient α_0 is a function of only one physical variable, namely the temperature T. However, ice exhibits an infrared absorption spectrum that includes a nonresonant term that varies as f. This led Hufford (1991) to propose the model[†]

$$\varepsilon_i'' = \frac{\alpha_0}{f} + \beta_0 f, \tag{4.24}$$

where α_0 and f are in GHz and β_0 is in $(\text{GHz})^{-1}$. As explained in detail by Mätzler (2006, pp. 456–460), the coefficients α_0 and β_0 are given by the semiempirical expressions

$$\alpha_0 = (0.00504 + 0.0062\theta)\cdot\exp(-22.1\theta) \quad \text{(GHz)}, \tag{4.25a}$$

$$\beta_0 = \frac{B_1}{T_K}\frac{\exp(b/T_K)}{[\exp(b/T_K)-1]^2} + B_2 f^2 + \exp[-9.963 + 0.0372(T_K - 273.16)] \quad (\text{GHz}^{-1}), \tag{4.25b}$$

[†]**Computer Code 4.3.**

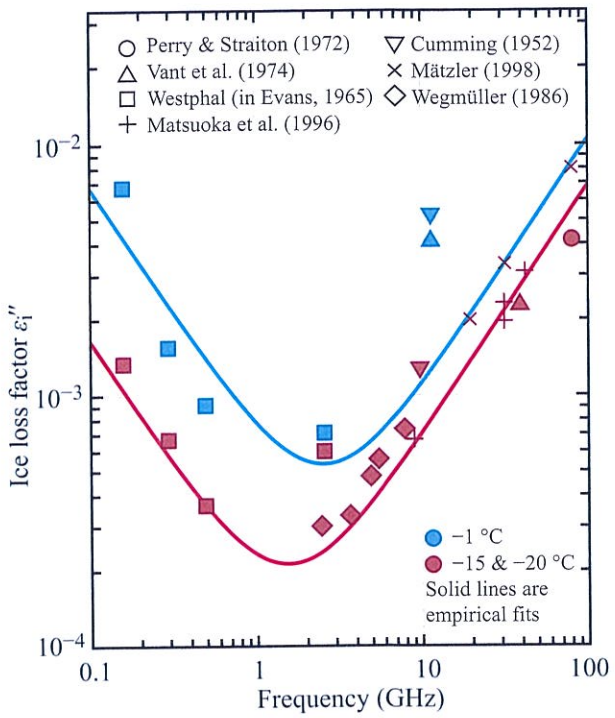

Figure 4-3: Loss factor of pure ice.

$$\theta = \frac{300}{T_K} - 1, \qquad T_K \text{ in K}, \tag{4.25c}$$

$$B_1 = 0.0207 \text{ K/GHz}, \quad b = 335 \text{ K},$$

and

$$B_2 = 1.16\times 10^{-11} \text{ GHz}^{-3}.$$

Figure 4-3 displays plots of the model for ε_i'' at 272 K (−1 °C) and 253 K (−20 °C). Also shown are data reported in the literature by various research groups. Both the data and the model exhibit a minimum in the neighborhood of 1 GHz. Some of the variability in the data is attributed to the difficulty associated with making accurate measurements of ε_i'' due to its small magnitude.

Fresh water ice often contains ionic impurities, such as dissolved salts, which causes its ε_i'' to increase significantly in comparison with that for pure ice. According to the data reported by Wegmüller (1986) and reproduced in Fig. 4-4, ε_i'' of an impure ice sample with $S = 13$ psu is 2–8 times larger than that of a

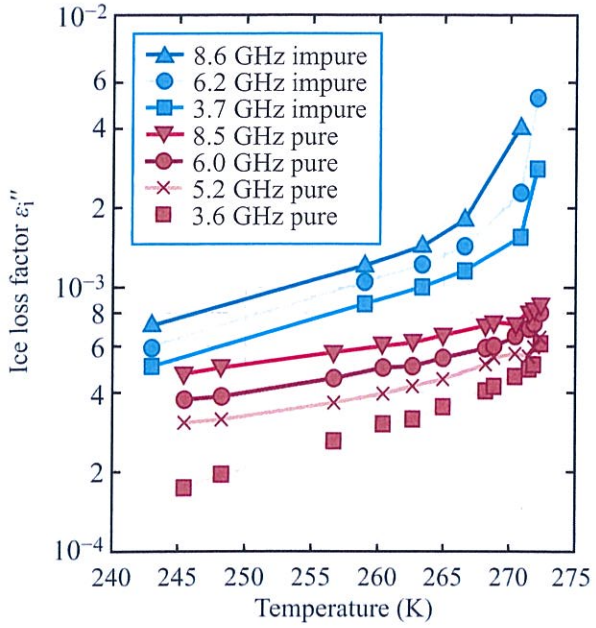

Figure 4-4: Loss factor ε_i'' of pure and slightly saline ($S = 13$ psu) ice as a function of temperature [Wegmüller, 1986].

pure ice sample; the relative increase depends on the temperature T, the frequency f, and the salinity S.

4-4 Dielectric Mixing Models for Heterogeneous Materials

The equivalent dielectric constant of a heterogeneous material (mixture) consisting of two or more substances is related to the dielectric constants of the individual substances, their volume fractions, their spatial distributions, and their orientations relative to the direction of the incident electric-field vector. Usually the substance with the highest volume fraction is regarded as the ***host material***, or continuous medium, and the other substances are regarded as ***inclusions***.

To relate the average dielectric constant of a mixture to the factors mentioned above, it is necessary to relate the average electric field (within the mixture as a whole) to the fields within the inclusions. If the inclusions are randomly dispersed within the host material, it is not possible to derive an exact solution for the fields within the inclusions because the mutual interactions of the inclusions (through their polarization fields) are dependent upon their positions relative to each other. Tinga and his associates (1973) provide a concise historical review of the various approximations proposed in the literature for solving the interaction problem, and Sihvola (1999) provides a comprehensive treatment of electromagnetic mixing formulas for computing the equivalent dielectric constant of a heterogeneous mixture. These approximations include (a) ignoring short-range interactions (between inclusions) altogether by restricting the validity of the dielectric mixing model to only those mixtures characterized by a low concentration of inclusions, (b) assigning an ***effective dielectric constant*** ε^* to the immediate surroundings of an included particle in an attempt to account for short-range interactions (de Loor, 1956; 1968), and (c) accounting for first-order inclusion interactions by solving Maxwell's equations with appropriate boundary conditions (Tinga et al., 1973). Also, *it is assumed in all cases that the dimensions of the inclusions are much smaller than the wavelength of the radiation propagating in the mixture medium*, thereby allowing the treatment to ignore volume scattering in the material.

4-4.1 Randomly Oriented Ellipsoidal Inclusions

A host material containing only one type of inclusion is called a ***two-phase mixture***. Consider the case where the inclusions are ellipsoidal particles of identical shape and size, randomly dispersed within the host material and randomly oriented with respect to the direction of the electric field of the incident wave. Each ellipsoid has dimensions $2a$, $2b$, and $2c$ along its major axes (Fig. 4-5), and the host and inclusion materials have isotropic dielectric constants ε_h and ε_i, respectively. The inclusion concentration is defined by the ***inclusion volume fraction*** v_i,

$$v_i = \frac{4}{3}\pi abcN, \qquad 0 \le v_i \le 1, \tag{4.26}$$

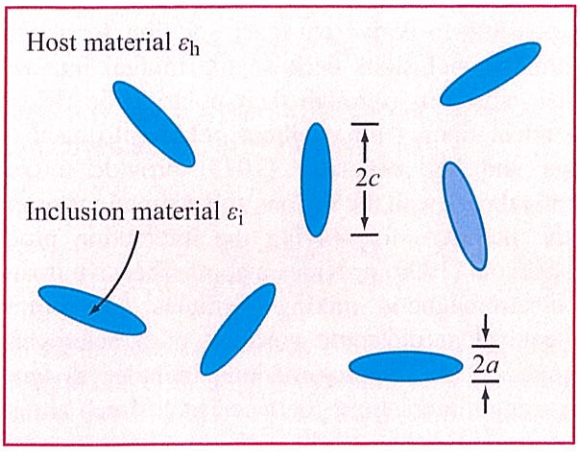

Figure 4-5: Randomly oriented ellipsoidal inclusions of identical size, shape, and dielectric constant ε_i, dispersed in a host material with dielectric constant ε_h. The ellipsoidal particles have semiaxes a, b, and c.

where N is the number of ellipsoids per m^3. The volume fraction of the host material is $v_h = 1 - v_i$.

4-4.2 Polder–van Santen/de Loor Formulas

Extending the early work of Polder and van Santen (1946) on the dielectrics of mixtures of solids, de Loor (1968) developed the following formula for the equivalent dielectric constant of a two-phase mixture containing randomly oriented ellipsoidal particles:

$$\varepsilon_m = \varepsilon_h + \frac{v_i}{3}(\varepsilon_i - \varepsilon_h) \sum_{u=a,b,c} \left[\frac{1}{1 + A_u \left(\frac{\varepsilon_i}{\varepsilon^*} - 1 \right)} \right], \tag{4.27}$$

where ε^* is an ***effective dielectric constant*** for the region immediately surrounding an included particle. For small inclusion volume fractions ($v_i \leq 0.1$), de Loor argues that short-range particle interactions may be ignored, in which case ε^* may be set equal to ε_h, the dielectric constant of the host material. For higher values of v_i, particle interactions may be accounted for, at least in part, by regarding the particle as being surrounded by the mixture rather than the host material. In that case, de Loor assigns $\varepsilon^* = \varepsilon_m$.

The quantity A_u inside the summation in Eq. (4.27) is the ***depolarization factor*** of the ellipsoid along its u axis ($u = a$, b, or c) and is given by (Landau and Lifshitz, 1975):

$$A_u = \frac{abc}{2} \int_0^\infty \frac{ds}{(s+u^2)[(s+a^2)(s+b^2)(s+c^2)]^{1/2}}, \quad u = a,\ b \text{ or } c. \tag{4.28}$$

The sum of the three depolarization factors is

$$A_a + A_b + A_c = 1. \tag{4.29}$$

For some specific ellipsoidal configurations of interest, the integral form of Eq. (4.28) can be simplified into closed-form solutions.

(a) A_u for Prolate Spheroids: For a prolate spheroid (needle-like) with $a = b$ (symmetric about the c axis) and $c > a$, Eq. (4.28) can be shown to lead to (Kerker, 1969)

$$A_c = \frac{1-e^2}{2e^3}\left[\ln\left(\frac{1+e}{1-e} \right) - 2e \right], \tag{4.30a}$$

$$A_a = A_b = \frac{1 - A_c}{2}, \tag{4.30b}$$

where e is the ellipsoid eccentricity,

$$e = \left[1 - \left(\frac{a}{c} \right)^2 \right], \qquad c > a. \tag{4.31}$$

(b) A_u for Spheres: For $a = b = c$,

$$A_a = A_b = A_c = \frac{1}{3}. \tag{4.32}$$

(c) A_u for Oblate Spheroids: For an oblate spheroid (disc-like) with $a = b$ and $c < a$, Eq. (4.28) has the closed-form solution

$$A_c = \frac{1}{e^2}\left[1 - \frac{(1-e^2)^{1/2}}{e} \sin^{-1} e \right], \tag{4.33a}$$

$$A_a = A_b = \frac{1 - A_c}{2}, \tag{4.33b}$$

where the eccentricity e of an oblate spheroid is defined as

$$e = \left[1 - \left(\frac{c}{a}\right)^2\right]^{1/2}, \qquad c < a. \tag{4.34}$$

Next, we consider Eq. (4.27) for specific shapes of inclusions.

(a) ε_m of Circular Disc Inclusions: For thin circular discs [Fig. 4-6(a)] with $a = b$ and $c \ll a$:

$$A_a = A_b = 0, \qquad A_c = 1, \tag{4.35a}$$

and Eq. (4.27) simplifies to

$$\varepsilon_m = \varepsilon_h + \frac{v_i}{3}(\varepsilon_i - \varepsilon_h)\left(2 + \frac{\varepsilon^*}{\varepsilon_i}\right). \tag{4.35b}$$

(b) ε_m of Spherical Inclusions: For spheres with $a = b = c$ [Fig. 4-6(b)]:

$$A_a = A_b = A_c \tag{4.36a}$$

and

$$\varepsilon_m = \varepsilon_h + 3v_i\varepsilon^* \frac{\varepsilon_i - \varepsilon_h}{\varepsilon_i + 2\varepsilon^*}. \tag{4.36b}$$

(c) ε_m of Needle Inclusions: For long, narrow needles [Fig. 4-6(c)] with $a = b$ and $c \gg a$:

$$A_a = A_b = 0.5, \qquad A_c = 0, \tag{4.37a}$$

and

$$\varepsilon_m = \varepsilon_h + v_i \frac{(\varepsilon_i - \varepsilon_h)(5\varepsilon^* + \varepsilon_i)}{3(\varepsilon_i + \varepsilon^*)}. \tag{4.37b}$$

► In all cases,

$$\varepsilon_m \to \varepsilon_h \text{ as } v_i \to 0,$$
$$\varepsilon_m \to \varepsilon_i \text{ as } v_i \to 1, \text{ if } \varepsilon^* = \varepsilon_m.$$

In the intermediate range, setting $\varepsilon^* = \varepsilon_h$ tends to underestimate the value of ε_m (when compared with experimental data) and setting $\varepsilon^* = \varepsilon_m$ tends to overestimate ε_m. ◄

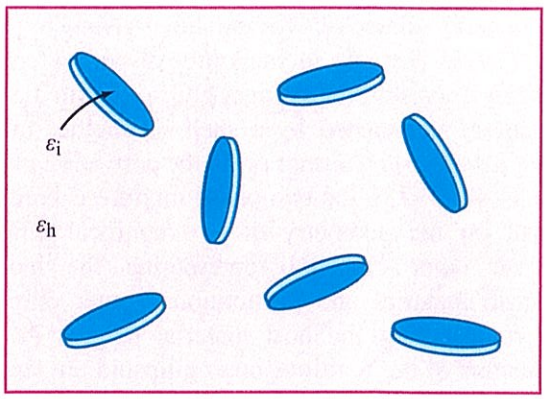

(a) Circular discs

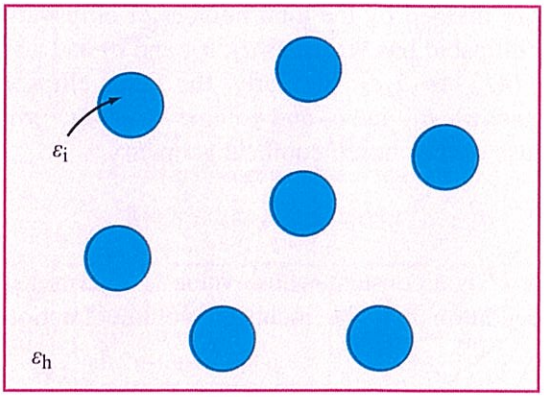

(b) Spheres

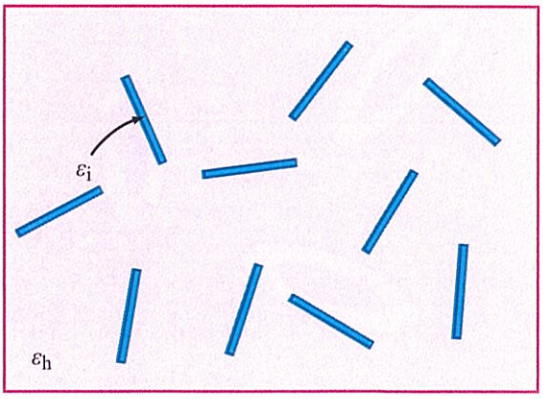

(c) Needles

Figure 4-6: Examples of randomly distributed ellipsoidal configurations.

4-4.3 Tinga-Voss-Blossey (TVB) Formulas

The general dielectric formulation given by Tinga et al. (1973) pertains to randomly dispersed confocal ellipsoids consisting of an inner ellipsoid with dielectric constant ε_i surrounded by a shell of another material having a dielectric constant ε_h. In the derivation given by Tinga et al. (1973), the two-phase mixture is compelled to take on the geometry of two confocal ellipsoids with an inner ellipsoid representing the inclusion dielectric material and a "fictitious" outer ellipsoidal shell representing the host material (Fig. 4-7). The dimensions of the fictitious outer ellipsoid are such that the volume of the shell surrounding the inner ellipsoid is equal to the total volume of the host material in the mixture divided by the total number of ellipsoids. The inner ellipsoid has semiaxes a_2, b_2, and c_2 and a volume $V_2 = (4/3)\pi a_2 b_2 c_2$; similarly, the outer ellipsoid has semiaxes a_1, b_1, and c_1 and volume $V_1 = (4/3)\pi a_1 b_1 c_1$. Because of the chosen confocal geometry,

$$a_1^2 - a_2^2 = b_1^2 - b_2^2 = c_1^2 - c_2^2 = k^2, \tag{4.38}$$

where k^2 is a constant whose value is determined from the condition that the inclusion volume fraction v_i is given by

$$v_i = \frac{V_2}{V_1}. \tag{4.39}$$

For randomly oriented inclusions, the equivalent dielectric constant of the two-phase mixture is given by†

$$\varepsilon_m = \varepsilon_h + \frac{v_i}{3}(\varepsilon_i - \varepsilon_h) \cdot \sum_{u=a,b,c} \frac{1}{1 + (A_{u2} - A_{u1} v_i)\left(\dfrac{\varepsilon_i}{\varepsilon_h} - 1\right)}, \tag{4.40}$$

where A_{u1} and A_{u2} are the depolarization factors of the outer and inner ellipsoids, respectively,

$$A_{u_j} = \frac{a_j b_j c_j}{2} \int_0^\infty \frac{ds}{(s+u_j^2)[(s+a_j^2)(s+b_j^2)(s+c_j^2)]^{1/2}}$$
$$u_j = a_j,\ b_j,\ \text{or}\ c_j;\quad j = 1 \text{ or } 2. \tag{4.41}$$

(a) ε_m of Circular Disc Inclusions: For thin circular discs with $a_1 = b_1$, $a_2 = b_2$, $c_1 \ll a_1$, and $c_2 \ll a_2$,

$$A_{a_1} = A_{a_2} = A_{b_1} = A_{b_2} = 0,$$
$$A_{c_1} = A_{c_2} = 1,$$

and

$$\varepsilon_m = \varepsilon_h + \frac{v_i}{3}(\varepsilon_i - \varepsilon_h)\left[\frac{2\varepsilon_i(1-v_i) + \varepsilon_h(1+2v_i)}{v_i\varepsilon_h + (1-v_i)\varepsilon_i}\right]. \tag{4.42}$$

(b) ε_m of Spherical Inclusions: For spheres,

$$A_{a_1} = A_{a_2} = A_{b_1} = A_{b_2} = A_{c_1} = A_{c_2} = \frac{1}{3}$$

and

$$\varepsilon_m = \varepsilon_h + \frac{3v_i\varepsilon_h(\varepsilon_i - \varepsilon_h)}{(2\varepsilon_h + \varepsilon_i) - v_i(\varepsilon_i - \varepsilon_h)}. \tag{4.43}$$

(c) ε_m of Needle Inclusions: For long, narrow needles,

$$A_{a_1} = A_{a_2} = A_{b_1} = A_{b_2} = 0.5,$$
$$A_{c_1} = A_{c_2} = 0,$$

and

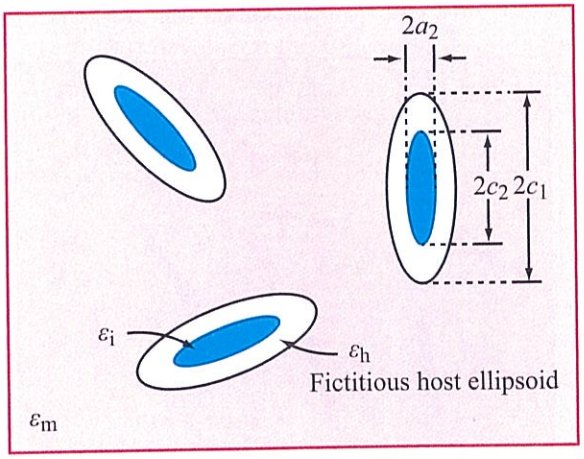

Figure 4-7: Two-phase confocal ellipsoidal TVB model (Tinga et al., 1973) in which each ellipsoidal inclusion is surrounded by a shell of host material whose thickness is governed by the volume fraction of the host material.

† **Computer Code 4.4.**

$$\varepsilon_m = \varepsilon_h + \frac{v_i}{3}(\varepsilon_i - \varepsilon_h)\left[\frac{\varepsilon_h(5+v_i)+(1-v_i)\varepsilon_i}{\varepsilon_h(1+v_i)+\varepsilon_i(1-v_i)}\right]. \quad (4.44)$$

▶ In all cases,

$$\varepsilon_m \to \varepsilon_h \text{ as } v_i \to 0,$$
$$\varepsilon_m \to \varepsilon_i \text{ as } v_i \to 1,$$

and the attractive feature of the ***Tinga-Voss-Blossey*** (TVB) model is that the unknown quantity, ε_m, is only on one side of the expressions given by Eqs. (4.42) to (4.44). ◀

Figure 4-8 displays plots for ε'_m and ε''_m as a function of the inclusion volume fraction v_i for spherical inclusions. The plots include the two de Loor formulas with $\varepsilon^* = \varepsilon_h$ and $\varepsilon^* = \varepsilon_m$ and the formula given by Eq. (4.43) based on the TVB model. The plots are for a host material with $\varepsilon_h = 1 - j0$ (air) and inclusions with $\varepsilon_i = 10 - j1$. The TVB model plot for ε'_m is intermediate between the two de Loor plots, and generally provides a better fit to experimental data. The same is true for ε''_m.

4-4.4 Other Dielectric Mixing Formulas

The literature contains numerous models and formulas for describing the dielectric behavior of mixtures. Comprehensive reviews are available in the paper by Tinga et al. (1973) and the books by Van Beek (1967) and Sihvola (1999). Most of these formulas are special cases of formulas given in earlier subsections.

We occasionally find it useful in forthcoming sections to use the formula

$$\varepsilon_m^\alpha = \varepsilon_h^\alpha + v_i(\varepsilon_i^\alpha - \varepsilon_h^\alpha), \quad (4.45)$$

where α is a constant. For $\alpha = 1$, the preceding formula is known as the ***linear model***, for $\alpha = 1/2$ as the ***refractive model*** (since $\varepsilon^{1/2} = n$ is the refractive index), and for $\alpha = 1/3$ as the ***cubic model***.

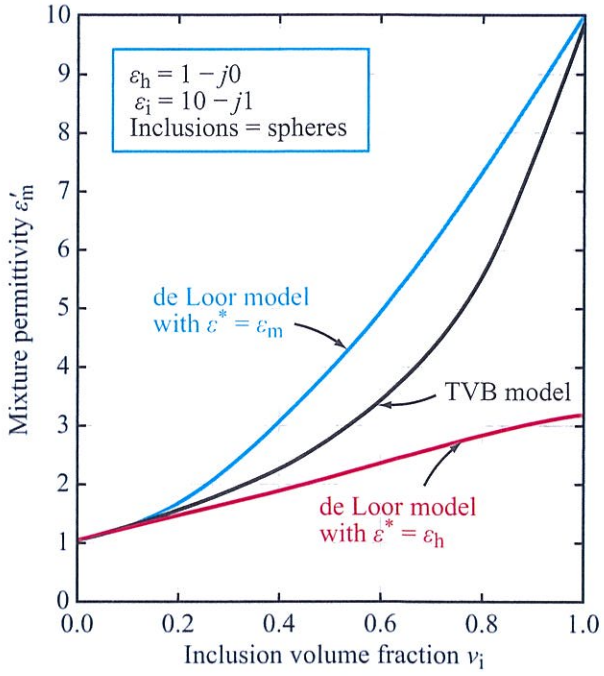

(a) Mixture permittivity ε'_m

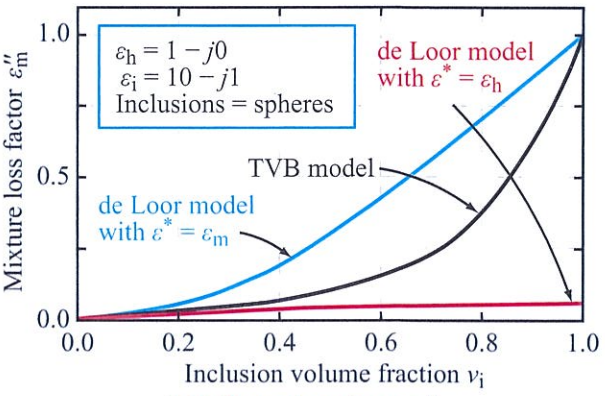

(b) Mixture loss factor ε''_m

Figure 4-8: Comparison of three dielectric mixing formulas for spherical inclusions.

4-5 Sea Ice

Sea ice is a much more complicated medium, both structurally and electromagnetically, than fresh-water ice. Sea ice is a heterogeneous mixture of liquid

brine inclusions and air pockets interspersed within the ice medium. The ***brine inclusions***, containing salt and water, exercise a strong influence on the complex dielectric constant of the mixture, because of their high complex-dielectric constant when compared with that of ice.

The growth rate of the ice layer governs both the shape and concentration of the brine inclusions. Sea ice generally is divided into three categories on the basis of age: (a) ***young ice***, which typically is less than 30 cm thick, (b) ***first-year ice***, whose thickness usually is between 30 cm and 2 m, and (c) ***multiyear ice***, whose thickness usually exceeds 2 m (Vant et al., 1978). The first two ice categories are similar in structure and often are treated as a single category. One of the major differences between multiyear ice and the other ice categories is their brine concentrations. A salinity profile of first-year ice typically decreases from about 5–16 psu near the surface to about 4–5 psu in the bulk of the ice and then increases rapidly to about 30 psu near the ice-water interface. In contrast, the salinity of multiyear ice usually is less than 1 psu in the surface layer and about 2–3 psu in the bulk portion. These values are representative of sea ice in the Arctic Ocean, where the salinity of liquid water is of the order of 32 psu. Close to land, the water's salinity can be much lower; in the Gulf of Finland, for example, the salinity of water is 6 psu and in the Gulf of Bothnia only 2 psu (Hallikainen, 1980). Sea-ice salinity in such areas is correspondingly lower than that of sea ice in arctic areas.

In general, the complex ***dielectric constant of sea ice***, ε_{si}, is a function of the following parameters: (a) the complex dielectric constant of pure ice, ε_i, (b) the complex dielectric constant of the brine pockets or inclusions, ε_b, (c) the ***fraction of brine by volume***, v_b, and (d) the shape and orientation of the brine pockets or inclusions relative to the direction of the electric field of the wave propagating in the ice medium. Indirectly, ε_{si} also is a function of the ice temperature T [through parameters (a)–(c)] and the ice salinity S_i (through v_b). Expressions and graphs for ε_i are available in Section 4-3. The other parameters are discussed next.

4-5.1 Dielectric Constant of Brine

Liquid brine is the same as saline water; therefore, the same basic expressions defining ε_w in Section 4-2 may be used to compute the complex dielectric constant of brine, ε_b, except for two modifications:

(1) The salinity of liquid brine is governed by its temperature. In sea ice, liquid brine exists in the form of pockets and inclusions, so a drop in temperature causes additional water to freeze, thereby increasing the brine-salt concentration. The ***brine salinity*** S_b (in psu) is related to the temperature T (°C) by the following empirical expressions (Assur, 1960; Poe et al., 1972):

$$\begin{aligned}
S_b &= 1.725 - 18.756T - 0.3964T^2, \\
&\quad -8.2 \le T \le -2°C; \\
S_b &= 57.041 - 9.929T - 0.16204T^2 - 0.002396T^3, \\
&\quad -22.9 \le T \le -8.2°C; \\
S_b &= 242.94 + 1.5299T + 0.0429T^2, \\
&\quad -36.8 \le T \le -22.9°C; \\
S_b &= 508.18 + 14.535T + 0.2018T^2, \\
&\quad -43.2 \le T \le -36.8°C.
\end{aligned} \tag{4.46}$$

A plot of S_b as a function of T is shown in Fig. 4-9.

The link between S_b and T means that the dielectric constant of brine ε_b is determined by the electromagnetic frequency f and the temperature T only.

(2) Some of the numerical expressions given in Section 4-2 were formulated with seawater in mind; therefore, they are not always applicable when salinities extend beyond 35 psu. Hence, the expressions developed by Stogryn (1971) for NaCl solutions are used instead because they cover the range $0 \le S \le 157$ psu. Even though sea-ice brine contains other salts in addition to NaCl, NaCl is the principal component; therefore, the expressions developed for pure NaCl solutions are assumed applicable. In terms of Stogryn's (1971) formulation, ε_b' and ε_b'' are given by

$$\varepsilon_b' = \varepsilon_{w\infty} + \frac{\varepsilon_{b0} - \varepsilon_{w\infty}}{1 + (2\pi f \tau_b)^2}, \tag{4.47a}$$

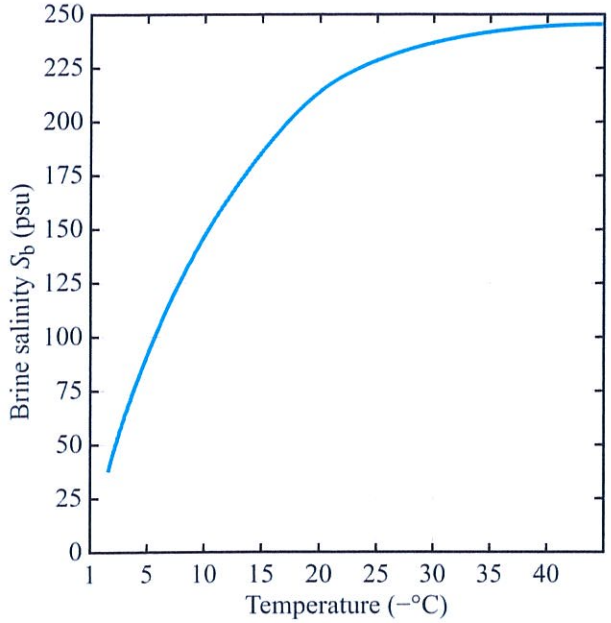

Figure 4-9: Brine salinity in sea ice as a function of negative temperature computed using Eq. (4.46).

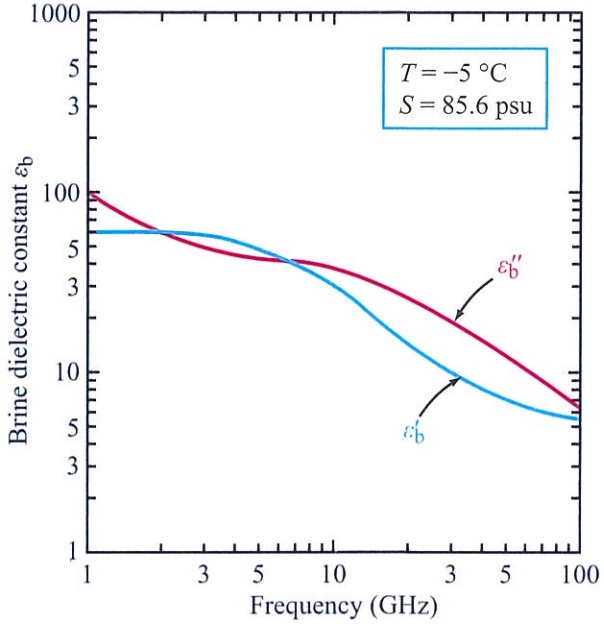

Figure 4-10: Dielectric constant of liquid brine as a function of frequency, calculated using the expressions in Section 4-5.1.

$$\varepsilon_b'' = (2\pi f \tau_b)\,\frac{(\varepsilon_{b0} - \varepsilon_{w\infty})}{1 + (2\pi f \tau_b)^2} + \frac{\sigma_b}{2\pi f \varepsilon_0}, \qquad (4.47b)$$

where $\varepsilon_{w\infty} = 4.9$,

$$\varepsilon_{b0}(T, N_b) = \varepsilon_{b0}(T, 0)\; a_1(N_b), \qquad (4.48a)$$

$$\tau_b(T, N_b) = \tau_b(T, 0)\; b_1(T, N_b), \qquad (4.48b)$$

$$\sigma_b(T, N_b) = \sigma_b(25, N_b)\; c_1(\Delta, N_b). \qquad (4.48c)$$

The preceding functions are given by the following expressions:

$\varepsilon_{b0}(T, 0) = \varepsilon_{w0}(T)$, as defined by Eq. (4.18),

$$a_1(N_b) = 1.0 - 0.255 N_b + 5.15 \times 10^{-2} N_b^2 - 6.89 \times 10^{-3} N_b^3, \qquad (4.49a)$$

$2\pi\tau_b(T, 0) = 2\pi\tau_w(T)$, as defined by Eq. (4.16),

$$b_1(T, N_b) = 1.0 + 0.146 \times 10^{-2} T N_b - 4.89 \times 10^{-2} N_b - 2.97 \times 10^{-2} N_b^2 + 5.64 \times 10^{-3} N_b^3, \qquad (4.49b)$$

$$\sigma_b(25, N_b) = N_b(10.39 - 2.378 N_b + 0.683 N_b^2 - 0.135 N_b^3 + 1.01 \times 10^{-2} N_b^4), \qquad (4.49c)$$

$$c_1(\Delta, N_b) = 1.0 - 1.96 \times 10^{-2}\Delta + 8.08 \times 10^{-5}\Delta^2 - N_b\Delta[3.02 \times 10^{-5} + 3.92 \times 10^{-5}\Delta + N_b(1.72 \times 10^{-5} - 6.58 \times 10^{-6}\Delta)], \qquad (4.49d)$$

$$N_b = S_b[1.707 \times 10^{-2} + 1.205 \times 10^{-5} S_b + 4.058 \times 10^{-9} S_b^2]. \qquad (4.49e)$$

In Eq. (4.49), N_b is the ***normality*** of the brine solution and $\Delta = (25 - T)$ in °C.

An example depicting the frequency dependence of ε_b' and ε_b'' is displayed in Fig. 4-10 for $T = -5$ °C. In comparison with the values discussed in the previous section for fresh-water ic, ε_b' is larger than ε_i' by more than an order of magnitude and ε_b'' is larger than ε_i'' by more than three orders of magnitude. Hence,

the presence of brine pockets and inclusions in ice can exercise a very strong influence on the dielectric properties of the mixture, even for very small values of the ***brine volume fraction*** v_b.

4-5.2 Brine Volume Fraction

The volume fraction of brine in sea ice is given by

$$v_b = \frac{S_i}{S_b}\frac{\rho_i}{\rho_b}, \tag{4.50}$$

where S_i and S_b are the salinities of the sea-ice mixture and of the brine component, respectively; ρ_i is the density of pure ice; and ρ_b is the density of the brine. As was indicated in the previous section, S_b is a function of the temperature T only. The brine density ρ_b also is temperature-dependent, although its relative sensitivity to T is much weaker than that of S_b. Using the experimental data reported by Assur in 1960, Frankenstein and Garner (1967) generated the following empirical expression:

$$v_b = 10^{-3} S_i \left(-\frac{49.185}{T} + 0.532\right), \tag{4.51}$$

$$-0.5°\text{C} \geq T \geq -22.9°\text{C},$$

where S_i is the salinity of the sea ice. Figure 4-11 is a plot of v_b/S_i for the above temperature range.

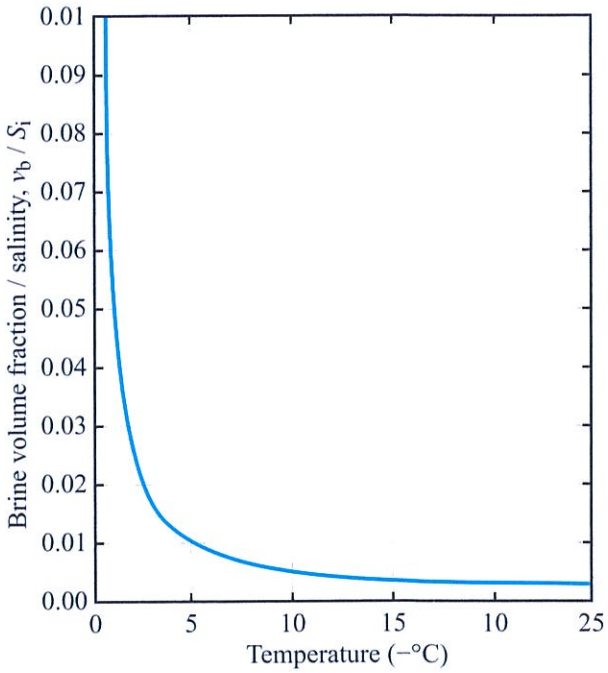

Figure 4-11: Plot of the ratio v_b/S_i (where S_i is in psu) as a function of negative temperature, based on Eq. (4.51).

4-5.3 Dielectric Properties

Due to the structural complexity and nonuniformity of sea ice, it has been difficult to measure its dielectric constant over a wide range of the governing parameters, namely the temperature T, brine volume fraction v_b and electromagnetic frequency f. These are in addition to the structural parameters, most notably the shapes and orientations of the brine inclusions. According to the review by Hallikainen (1992), measurements had been conducted at several frequencies between 0.1 GHz and 40 GHz, but most were at frequencies below 10 GHz. Some of the ice samples were simulated under laboratory conditions while others were extracted from natural sea ice in the Bering Sea and the Beaufort Sea. In view of all of these factors, no credible model exists for the dielectric constant of sea ice, so our approach in the present section is to present selected samples of reported experimental data so as to give the reader an overview, albeit incomplete, of the dielectric behavior of sea ice.

Variation with T

► According to measured data, the real part of the dielectric constant of sea ice, ε'_{si}, varies with several sea-ice parameters; however, over the 1 to 40 GHz range it appears to be bounded within the range $2.5 \leq \varepsilon'_{si} \leq 8$. ◄

The temperature dependence of ε_{si} is illustrated in Figs. 4-12 and 4-13 (from Vant et al., 1974) for three types of ice: (a) frazil ice, which usually comprises the top layer of first-year ice and is characterized by spherical brine pockets, (b) columnar ice, which usually

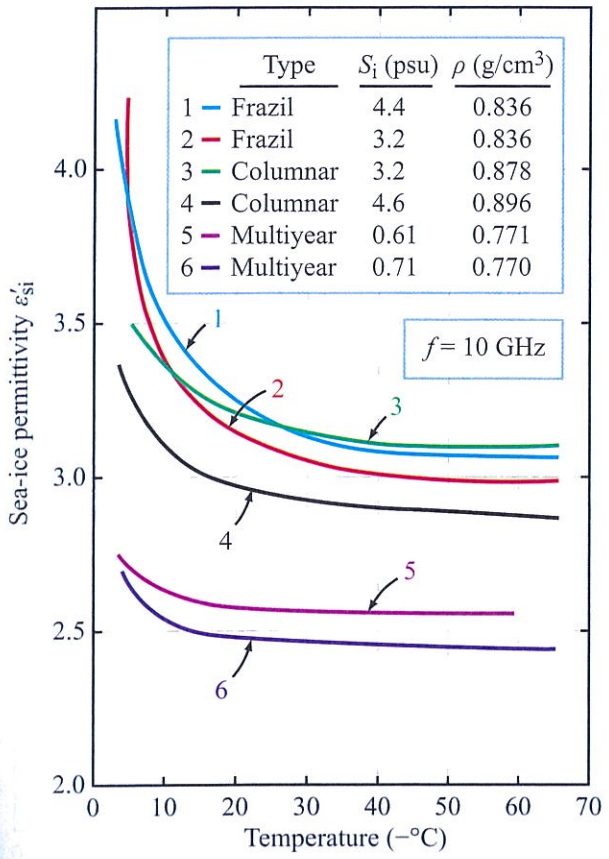

Figure 4-12: Temperature variation of the permittivity of three types of sea ice at 10 GHz [from Vant et al., 1974].

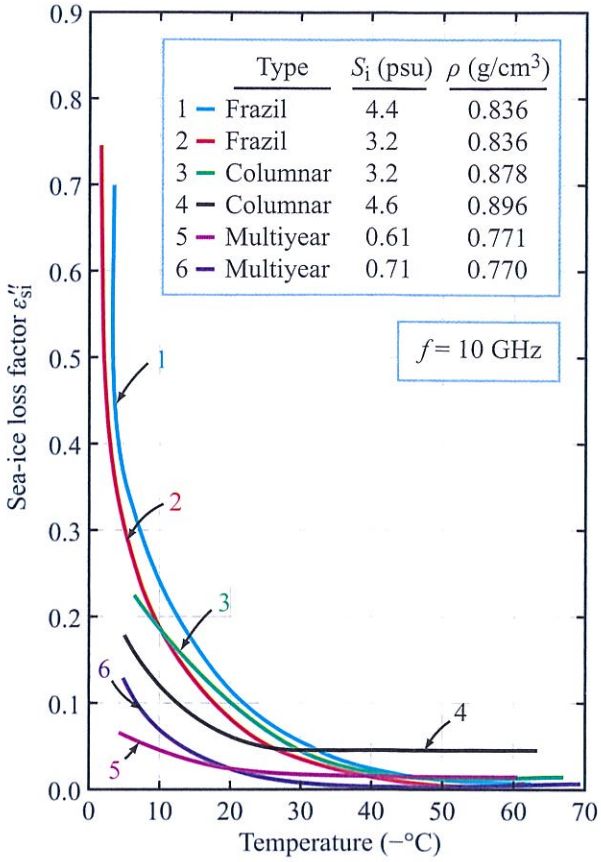

Figure 4-13: Temperature variation of the loss factor for three types of sea ice at 10 GHz [Vant et al., 1974].

occurs beneath a layer of frazil ice in first-year ice and is characterized by elongated brine pockets, and (c) multiyear ice. In Fig. 4-14, dielectric data reported by various investigators through 1992 are grouped into frequency bands: (a) 0.9–1 GHz, (b) 4–4.75 GHz, and (c) 9.5–16 GHz.

Variation with v_b

In their investigation of the dielectric properties of laboratory-simulated sea ice, Arcone et al. (1986) examined the dependence of ε'_{si} and ε''_{si} on the brine volume fraction v_b over a wide range extending between 5 psu and 100 psu. The ice was grown from water with a salinity in the 23–25 psu range, which is characteristic of first-year sea ice. Their results, measured at 4.75 GHz, are shown in Fig. 4-15. We observe that ε'_{si} increases by a factor of about 30% as v_b is increased from about zero to 100 psu, but this rate of increase pales by comparison with that for ε''_{si}, which increases by more than two orders of magnitude (ε''_i of pure ice at 4.75 GHz is on the order of 3×10^{-4}, compared with $\varepsilon''_{si} \approx 0.5$ at $v_b = 100$ psu).

Differences in the propagation properties of pure ice and sea ice may be illustrated through a comparison of their attenuation coefficients. At 10 GHz, the attenuation coefficient of pure (fresh-water) ice, α_i, is on the order of 1 dB m^{-1}. In contrast, the attenuation

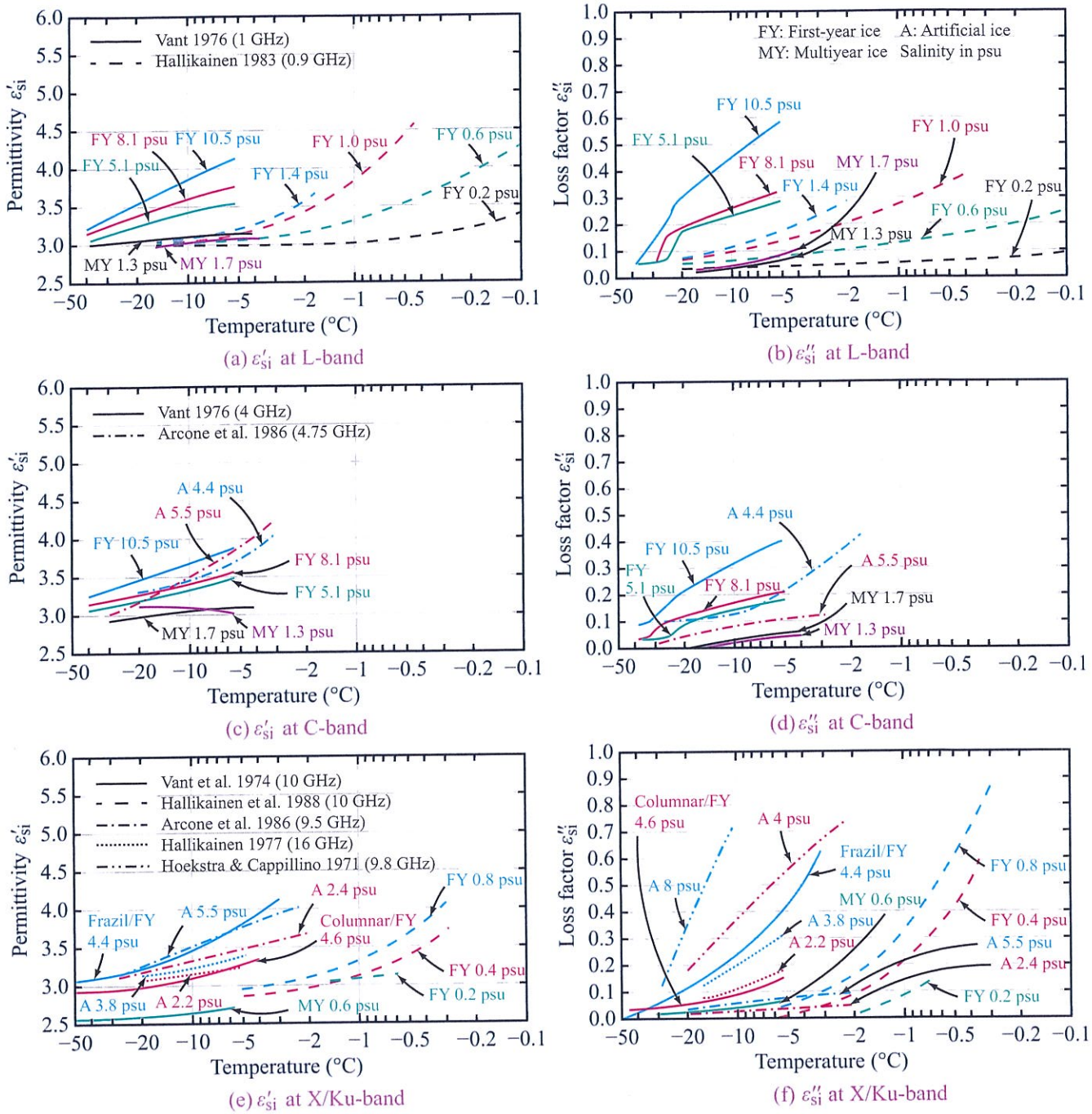

Figure 4-14: Measured permittivity and loss factor of sea ice at L-, C-, and X/Ku-bands [Hallikainen, 1992].

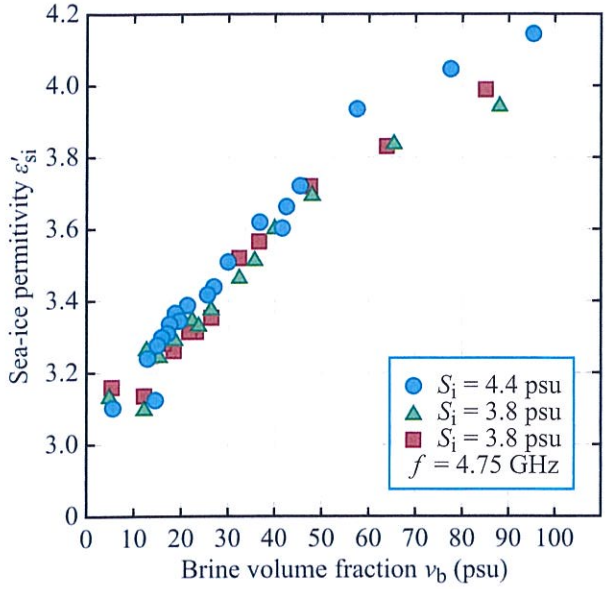

(a) Sea-ice permitivity ε'_{si}

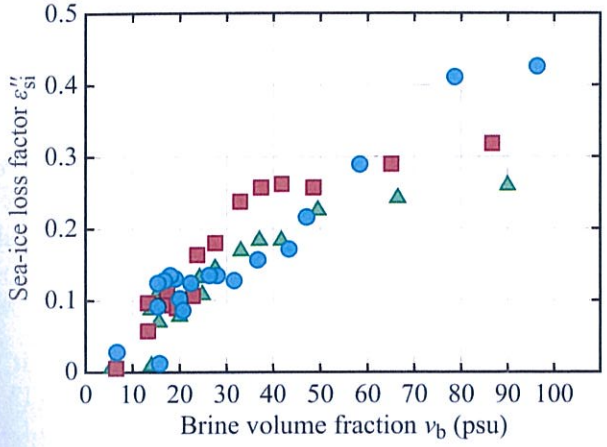

(b) Sea-ice loss factor ε''_{si}

Figure 4-15: Measured permittivity and loss factor of simulated sea ice at 4.7 GHz, plotted as a function of brine volume fraction [Arcone et al., 1986].

coefficient of sea ice may reach values in excess of 200 dB m^{-1}, depending upon the temperature and salinity of the ice (Finkelstein et al., 1970; Glushnev et al., 1976). This point may be illustrated further

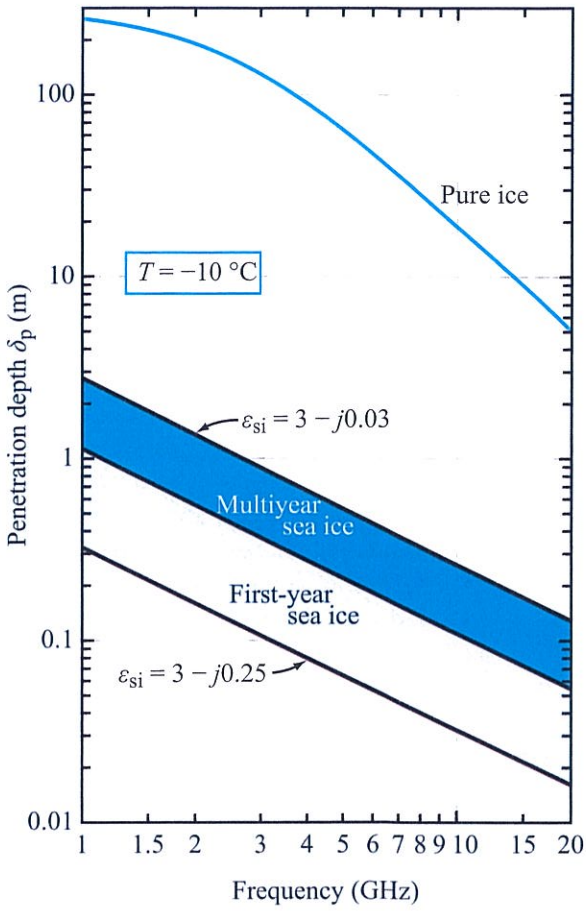

Figure 4-16: Calculated penetration depth for pure ice, first-year sea ice, and multiyear sea ice.

by using the curves shown in Fig. 4-16, which depict the spectral variation of the penetration depth δ_p at $T = -10$ °C for representative cases of pure ice, first-year ice, and multiyear ice. The curves were calculated using Eq. (4.12) as follows:

(a) For pure ice, $\varepsilon'_i = 3.18$ at $T = -10$ °C and it is independent of frequency; ε''_i is given graphically in Fig. 4-3 for $T = -1$ °C and -20 °C. Assuming an approximately linear temperature dependence, the values of ε''_i at $T = -10$ °C were obtained by interpolation between the two curves.

(b) For first-year ice at $T = -10$ °C, the dielectric constant was taken to be $\varepsilon_{si} = 3.3 - j0.25$. The real part was chosen on the basis of Fig. 4-12, which shows that ε'_{si} of first-year ice varies between 3.1 and 3.5 at -10 °C. According to Fig. 4-13, the imaginary part of the relative dielectric constant of first-year ice varies between 0.1 and 0.25 (at 10 GHz and $T = -10$ °C for the cases shown). The bottom curve in Fig. 4-16 is intended to represent a high-loss example of first-year ice. Hence, $\varepsilon''_{si} = 0.25$ was chosen as a representative value for this case. Additionally, in view of the fact that no consistent, discernible frequency dependence has been observed over the 1–20 GHz region for the dielectric constant of "natural" sea ice, the 10 GHz values of ε_{si} noted above were assumed to be representative of the 1–20 GHz frequency range. The curve defining the upper boundary of the shaded area denoted as "first-year sea ice" in Fig. 4-16 corresponds to a dielectric constant $\varepsilon_{si} = 3 - j0.07$, which is taken to be representative of the boundary between first-year and multiyear sea-ice conditions.

(c) The shaded area in Fig. 4-16 corresponding to "multiyear sea ice" is bounded by curves calculated for $\varepsilon_{si} = 3 - j0.07$ and $\varepsilon_{si} = 3 - j0.03$. The imaginary parts were based on Fig. 4-13.

The curves for ε_{si} given in this section clearly show that both ε'_{si} and ε''_{si} decrease rapidly with increasing negative temperature for the temperature range between 0 °C and -10 °C, and decrease at a lower rate at higher negative temperatures. Moreover, the normalized temperature sensitivity of the real part, $|\partial\varepsilon'_{si}/\partial T|/\varepsilon'_{si}$, is several times smaller in magnitude than the normalized temperature sensitivity of the imaginary part, $|\partial\varepsilon''_{si}/\partial T|/\varepsilon''_{si}$. This means that the penetration depth, $\delta_p \approx \sqrt{\varepsilon'_{si}}\,(k_0\varepsilon''_{si})^{-1}$, increases with increasing negative temperature. Thus, if the curves in Fig. 4-16 for first-year and multiyear sea ice at $T = -10$ °C are used as a reference, the corresponding values of δ_p at temperatures closer to 0 °C are 2 to 3 times smaller and values at -30 °C are 3 to 10 times larger.

4-6 Dielectric Constant of Snow

We divide our treatment of the dielectric properties of snow into two subsections, one for ***dry snow***, which is a mixture of ice and air and contains no free (liquid) water, and ***wet snow***, which does contain free water.

4-6.1 Dry Snow

The dielectric constant of dry snow, $\varepsilon_{ds} = \varepsilon'_{ds} - j\varepsilon''_{ds}$, depends on three quantities: (a) the dielectric constant of air, $\varepsilon_{air} = 1 - j0$, (b) the dielectric constant of ice, $\varepsilon_i = \varepsilon'_i - j\varepsilon''_i$, and the ice volume factor v_i. The volume fraction of ice in snow is related to the ***snow density*** ρ_s (in g/cm^3) through

$$v_i = \frac{\rho_s}{0.9167}\,, \tag{4.52}$$

where 0.9167 g/cm^3 is the density of pure ice.

Permittivity of dry snow

As was noted in Section 4-3 in connection with Eq. (4.23), ε'_i of ice is independent of frequency across the entire microwave band and its temperature sensitivity is so small as to be ignored. Hence, we assign it the value

$$\varepsilon'_i = 3.17,$$

which corresponds to Eq. (4.23) at $T = -20$ °C. If we use $\varepsilon_h = 1$ (for air) in the Tinga-Voss-Blossey (TVB) model for spherical inclusions given by Eq. (4.43), we obtain the following expression for the dielectric constant of the mixture, which now is dry snow,

$$\varepsilon_{ds} = 1 + \frac{3v_i(\varepsilon_i - 1)}{(2 + \varepsilon_i) - v_i(\varepsilon_i - 1)}\,, \tag{4.53}$$

where $\varepsilon_i = \varepsilon'_i - j\varepsilon''_i$ is the dielectric constant of ice. Our goal is to derive a single, but fairly accurate, expression for ε'_{ds}. Since $\varepsilon''_i \ll \varepsilon'_i$, we ignore ε''_i altogether and we use $\varepsilon_i = 3.17$ in Eq. (4.53). The result is

$$\varepsilon'_{ds} \approx \frac{1 + 0.84v_i}{1 - 0.42v_i}\,. \tag{4.54}$$

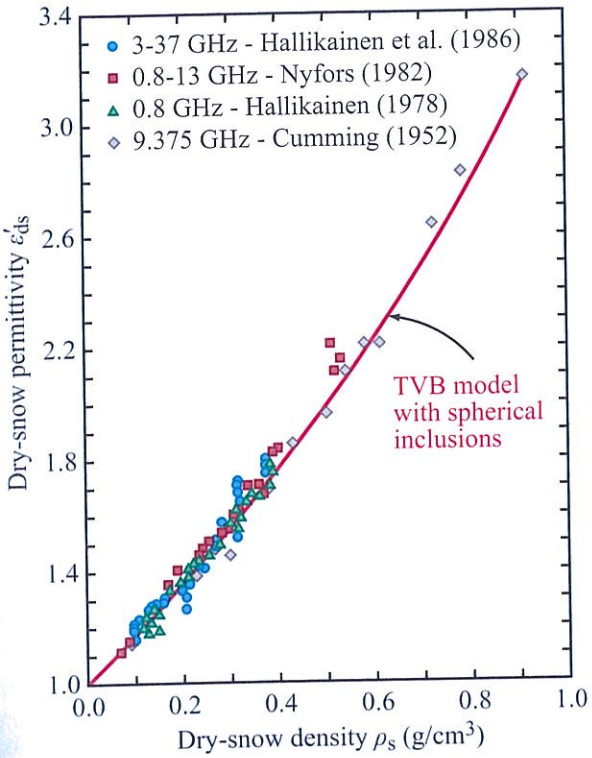

Figure 4-17: Measured permittivity of dry snow as a function of snow density.

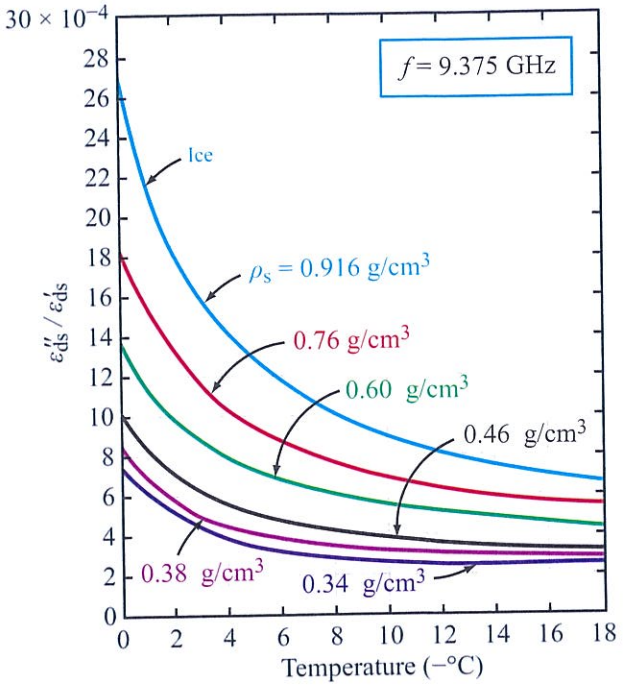

Figure 4-18: The loss tangent of dry snow as a function of temperature at a frequency of 9.375 GHz [from Cumming, 1952].

For $v_i = 0$ (pure air), $\varepsilon'_{ds} = 1$; and for $v_i = 1$ (pure ice), $\varepsilon'_{ds} = 3.17$, thereby confirming that the formula predicts the correct values at the two extreme values of v_i. Figure 4-17 shows a plot of Eq. (4.54), together with experimental measurements of ε'_{ds} made over a wide frequency range extending from 0.8 GHz to 37 GHz. The TVB model represented by Eq. (4.54) provides a good fit to the experimental data.

An equally good fit to the data is provided by the empirical expression (Mätzler, 2006)†

$$\varepsilon'_{ds} = \begin{cases} 1 + 1.4667 v_i + 1.435 v_i^3 & \text{for } 0 \le v_i \le 0.45, \\ (1 + 0.4759 v_i)^3 & \text{for } v_i \ge 0.45. \end{cases} \tag{4.55}$$

†Computer Code 4.5.

Loss factor of dry snow

As was stated earlier, ε'_{ds} is essentially independent of both temperature and frequency in the microwave region. In contrast, the loss factor of dry snow ε''_{ds} is strongly dependent on both parameters. The family of plots in Fig. 4-18 depict the variation of $\varepsilon''_{ds}/\varepsilon'_{ds}$ as a function of negative temperature at 9.375 GHz, with ρ_s as a parameter. The variation of $\varepsilon''_{ds}/\varepsilon'_{ds}$ with frequency is shown in Fig. 4-19, based on measurements from 0.8 GHz to 12.6 GHz. The family of plots exhibits a minimum in the 1–2 GHz range, similar to the minimum exhibited by ε''_i of ice in Fig. 4-3. Since dry snow is a mixture of ice and air, ε''_{ds} should mimic the temperature and frequency behavior of ε''_i. To obtain a model expression for $\varepsilon''_{ds}/\varepsilon''_i$, we proceed as follows:

(1) In the TVB model expression given by Eq. (4.53), we set $\varepsilon_{ds} = \varepsilon'_{ds} - j\varepsilon''_{ds}$ and $\varepsilon_i = \varepsilon'_i - j\varepsilon''_i$.

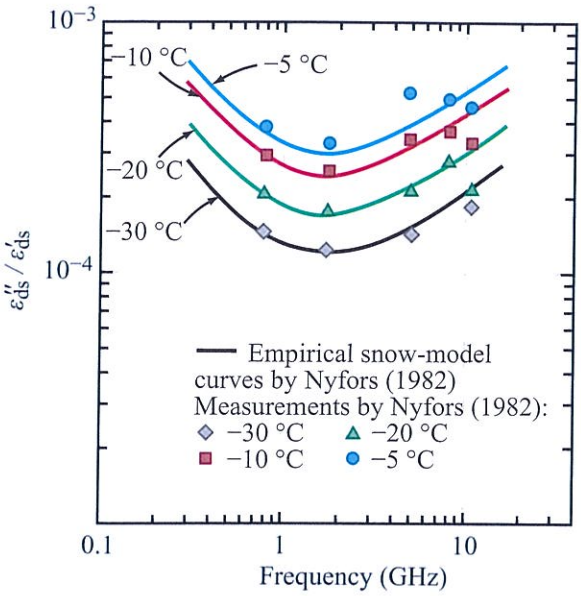

Figure 4-19: The loss tangent of dry snow as a function of frequency with temperature as parameter. Snow density is 0.45 g/cm^3 [from Nyfors, 1982].

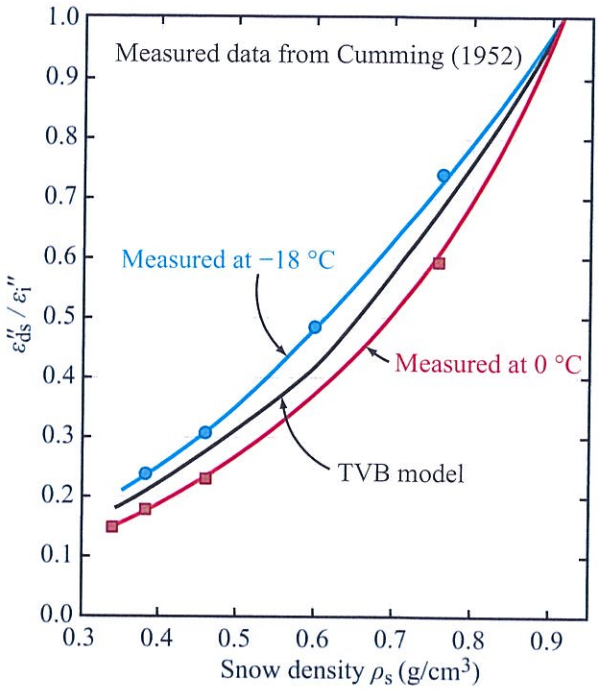

Figure 4-20: Comparison of Eq. (4.57) with measured data.

(2) We multiply the numerator and denominator of the second term on the right-hand side of the equation by the complex conjugate of its denominator so as to obtain an expression of the form $\varepsilon'_{ds} - j\varepsilon''_{ds} = a - jb$.

(3) We then equate ε''_{ds} to the term b, and we simplify it by ignoring terms of small magnitude when appropriate.

The process leads to (Hallikainen et al., 1986):

$$\varepsilon''_{ds} = \frac{9v_i\varepsilon''_i}{[(2+v_i)+\varepsilon'_i(1-v_i)]^2}\,. \qquad (4.56)$$

Upon setting $\varepsilon'_i = 3.17$, the expression simplifies to

$$\varepsilon''_{ds} = \frac{0.34v_i\varepsilon''_i}{(1-0.42v_i)^2}\,. \qquad (4.57)$$

A plot of $\varepsilon''_{ds}/\varepsilon''_i$ as a function of ρ_s is shown in Fig. 4-20. Also shown are plots extracted from Fig. 4-18 for $T = 0$ °C and -18 °C. The theoretical curve due to the TVB model is intermediate between the 0 °C and -18 °C data curves. According to Eq. (4.57), $\varepsilon''_{ds}/\varepsilon''_i$ should be temperature-independent, which means that the 0 °C and -18 °C plots should be identical. The fact that they are not is attributed to measurement inaccuracy.

To determine ε''_{ds} from Eq. (4.57), we need to know the value of ε''_i of the ice from which the snow is made with a reasonable degree of accuracy. As noted earlier in connection with Fig. 4-4, ε''_i can vary significantly with the amount of impurity present in the ice; a salinity as low as 1 psu is sufficient to cause ε''_i to double in value. To reconcile the data in Figs. 4-18 and 4-19 with the model given by Eq. (4.57), it is necessary to use values for ε''_i that are multiple times those reported for pure ice in Fig. 4-3.

4-6.2 Wet Snow

In the proximity of 0 °C, snow can support water in liquid form. Because of the high dielectric constant

of liquid water compared with that of air and ice, the presence of liquid water strongly affects the dielectric constant of the snow mixture. The liquid-water content of snow (or ***snow wetness***) m_v is the volume fraction of liquid water in the snow mixture, and usually it is expressed as a percentage. Occasionally snow wetness is expressed as a percentage of liquid water by weight, w_w. These two quantities are related by the approximate expression $m_v = w_w \rho_{ws}$, where ρ_{ws} is the density of wet snow, which is approximately equal to the density of dry snow ρ_s because the densities of water (1 g/cm^3) and pure ice (0.9167 g/cm^3) are fairly close to one another.

An extensive investigation of the dielectric behavior of natural snow was conducted by Hallikainen et al. (1983, 1984, 1986) using a free-space transmission technique. The permittivity and the dielectric loss factors of wet snow, ε'_{ws} and ε''_{ws}, were measured for 110 snow samples at nine frequencies between 4 and 18 GHz. Of these, 62 samples were also measured at 3 GHz and 37 GHz. Thus, although their results cover the range between 3 and 37 GHz, they are more heavily influenced by the 4–18 GHz measurements. The range of m_v covered by the samples extended between 1 and 12 percent. The measurement apparatus employed a pair of horn antennas used for transmission and reception and was arranged for wave propagation along the vertical direction. By operating the apparatus from a location adjacent to a snow-covered field, it was possible to remove snow slabs from the field while causing minimal disturbance to the snow's geometry. Each slab—approximately 50 cm in diameter, a few centimeters thick, and supported by a thin styrofoam sheet—was placed between the two antennas in order to measure the amplitude and phase of its transmission coefficient (from which ε'_{ws} and ε''_{ws} were determined).

In addition to measuring the complex dielectric constant of wet snow ($m_v > 1\%$), Hallikainen et al. (1986) measured the permittivity of dry snow for the range of snow density between 0.09 and 0.38 g/cm^3. The following linear fit to the data was obtained:

$$\varepsilon'_{ds} = 1.0 + 1.832\rho_s, \tag{4.58}$$

with a linear correlation coefficient of 0.96 and an rms error of 0.04.

When they analyzed the dielectric measurements for wet snow, Hallikainen et al. found that the analysis became simpler when the dependence of ε'_{ws} on snow density was (approximately) removed through conversion to the incremental permittivity $\Delta\varepsilon'_{ws}$,

$$\Delta\varepsilon'_{ws} = \varepsilon'_{ws} - 1.0 - 1.832\rho_s. \tag{4.59}$$

This is not the case for the dielectric loss factor ε''_{ws} because it is almost entirely an incremental quantity introduced by the presence of liquid water.

Typical examples of the variations of $\Delta\varepsilon'_{ws}$ and ε''_{ws} with m_v are shown in Fig. 4-21. The data points are based on measurements of ε'_{ws} and ε''_{ws}, whereas the solid curve was calculated using an empirical, modified ***Debye-like model*** given by[†]

$$\varepsilon'_{ws} = A + \frac{Bm_v^x}{1 + (f/f_0)^2}, \tag{4.60a}$$

$$\varepsilon''_{ws} = \frac{C(f/f_0)m_v^x}{1 + (f/f_0)^2}, \tag{4.60b}$$

where f_0 is an effective relaxation frequency of wet snow. The constants A, B, C, f_0, and x were determined by fitting 955 measurements for ε'_{ws}, and an identical number for ε''_{ws}, to the above expressions. The results, which pertain to the ranges $3 \le f \le 37$ GHz, $0.09 \le \rho_s \le 0.38$ g/cm^3, and $1 \le m_v \le 12\%$, are

$$A = A_1(1.0 + 1.83\rho_s + 0.02m_v^{1.015}) + B_1, \tag{4.61a}$$

$$B = 0.073A_1, \tag{4.61b}$$

$$C = 0.073A_2, \tag{4.61c}$$

$$x = 1.31, \tag{4.61d}$$

$$f_0 = 9.07 \text{ GHz}, \tag{4.61e}$$

$$A_1 = 0.78 + 0.03f - 0.58 \times 10^{-3} f^2, \tag{4.61f}$$

$$A_2 = 0.97 - 0.39f \times 10^{-2} + 0.39 \times 10^{-3} f^2, \tag{4.61g}$$

$$B_1 = 0.31 - 0.05f + 0.87 \times 10^{-3} f^2, \tag{4.61h}$$

where f is in GHz. The importance of the frequency-dependent constants is primarily at frequencies above

[†] **Computer Code 4.6.**

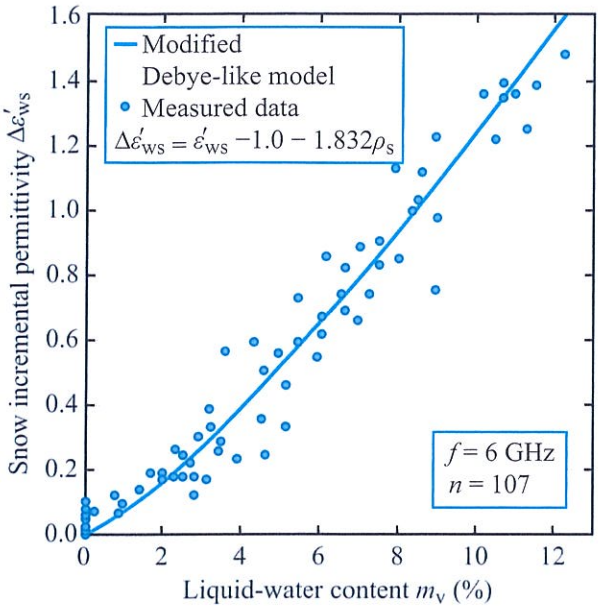

(a) Incremental permittivity

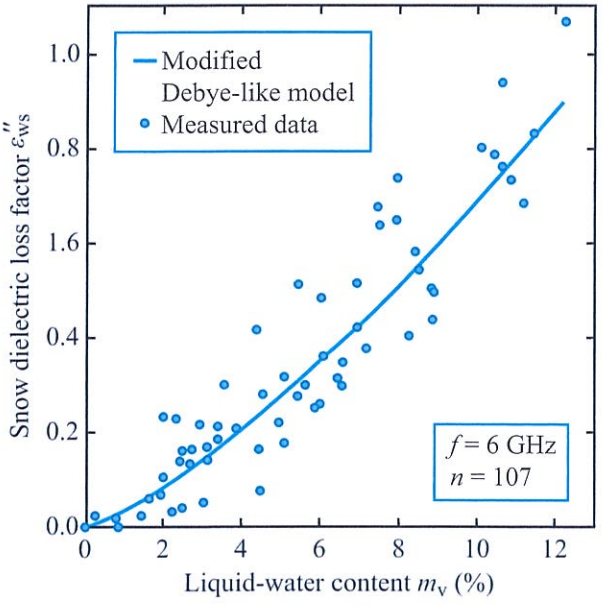

(b) Loss factor

Figure 4-21: Real and imaginary parts of the relative dielectric constant of snow as a function of liquid-water content at 6 GHz [from Hallikainen et al., 1986].

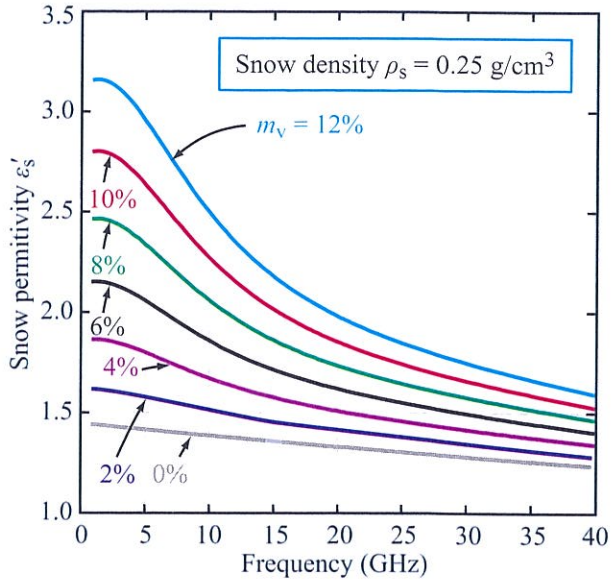

Figure 4-22: Spectral variation of the permittivity of wet snow with snow wetness as a parameter. The plots are based on the modified Debye-like model given by Eq. (4.60).

15 GHz; below 15 GHz we may set $A_1 = A_2 = 1.0$ and $B_1 = 0$.

The value of f_0 is slightly higher than the relaxation frequency of water at 0 °C, $f_0 = 8.9$ GHz. This is in agreement with the results of previous studies concerning heterogeneous mixtures containing water. Both theoretically and experimentally, de Loor (1968) found that the relaxation frequency of such mixtures is always equal to or higher than that of the relaxing component.

The curves shown in Fig. 4-21, which were calculated using the expressions given by Eq. (4.60) for $f = 6$ GHz, appear to provide a reasonable fit to the data for both $\Delta\varepsilon'_{ws}$ and ε''_{ws}. For the data-set as a whole, Hallikainen et al. (1986) evaluated the linear correlation coefficients between the measured and calculated values of the dielectric constant of snow, and found them to be on the order of 0.99 for $\Delta\varepsilon'_{ws}$ and 0.98 for $\Delta\varepsilon''_{ws}$.

Figures 4-22 to 4-24 show the effect of liquid-water content on the dielectric behavior of wet snow between

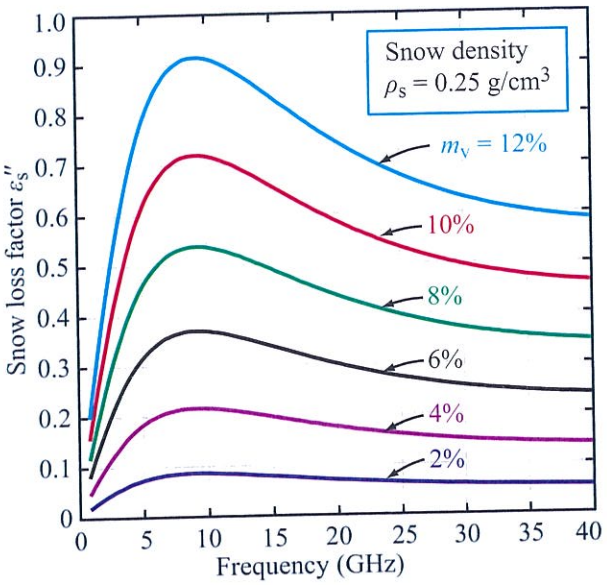

Figure 4-23: Spectral variation of the loss factor of wet snow with wetness as a parameter. The plots are based on the modified Debye-like model given by Eq. (4.60).

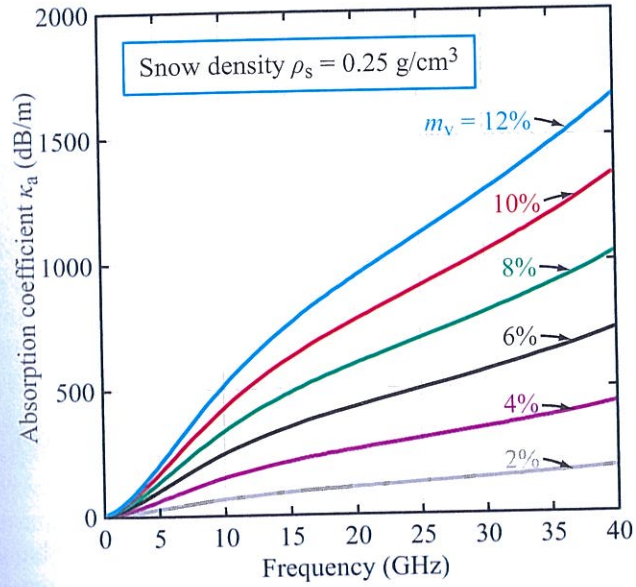

Figure 4-24: Spectral variation of the attenuation coefficient of wet snow with wetness as a parameter. The curves are based on the modified Debye-like model.

3 GHz and 37 GHz. The results are shown for a dry snow density $\rho_{ds} = 0.25$ g/cm^3, which was the average observed value during this study. The values of ε'_{ws} and ε''_{ws} were calculated using the modified Debye-like equations (4.60) and (4.61). As shown in Fig. 4-23, ε''_{ws} reaches its maximum value at 9.0 GHz. This agrees with the relaxation frequency of water at 0 °C. The sharp increase in ε''_{ws} between 3 GHz and 6 GHz is due to the large increase in the magnitude of ε''_w for water over this frequency range. The attenuation constant of wet snow increases practically linearly with frequency up to 15 GHz. Between 18 GHz and 37 GHz, the average slope is slightly smaller.

4-7 Dielectric Constant of Dry Rocks

An extensive study of the dielectric properties of rocks and powders was conducted by Campbell and Ulrichs (1969), in which they made measurements of 36 types of rocks, in both solid and powder forms, at 450 MHz and 35 GHz. Two decades later, several measurement techniques were used to investigate the dielectric properties of 80 rock samples across the 0.5–18 GHz range (Ulaby et al., 1990a). A summary of the results of these two studies follows.

4-7.1 Powdered Rocks

The bulk density of rocks, ρ_b in g/cm^3, varies between 1 g/cm^3 for rock material crushed into powder form to about 3.4 for some high density rocks like peridotites. The data set reported by Campbell and Ulrichs (1969) included dielectric measurements for 25 different types of powdered rocks, all at a density of 1 g/cm^3.

▶ Their results show that the relative permittivity ε'_p of the powdered rocks varied over a narrow range between 1.9 and 2.1, with a mean value around 2.0. Thus, when normalized to the same density, all rocks have approximately the same permittivity $\varepsilon'_p \approx 2.0$, regardless of rock type. ◀

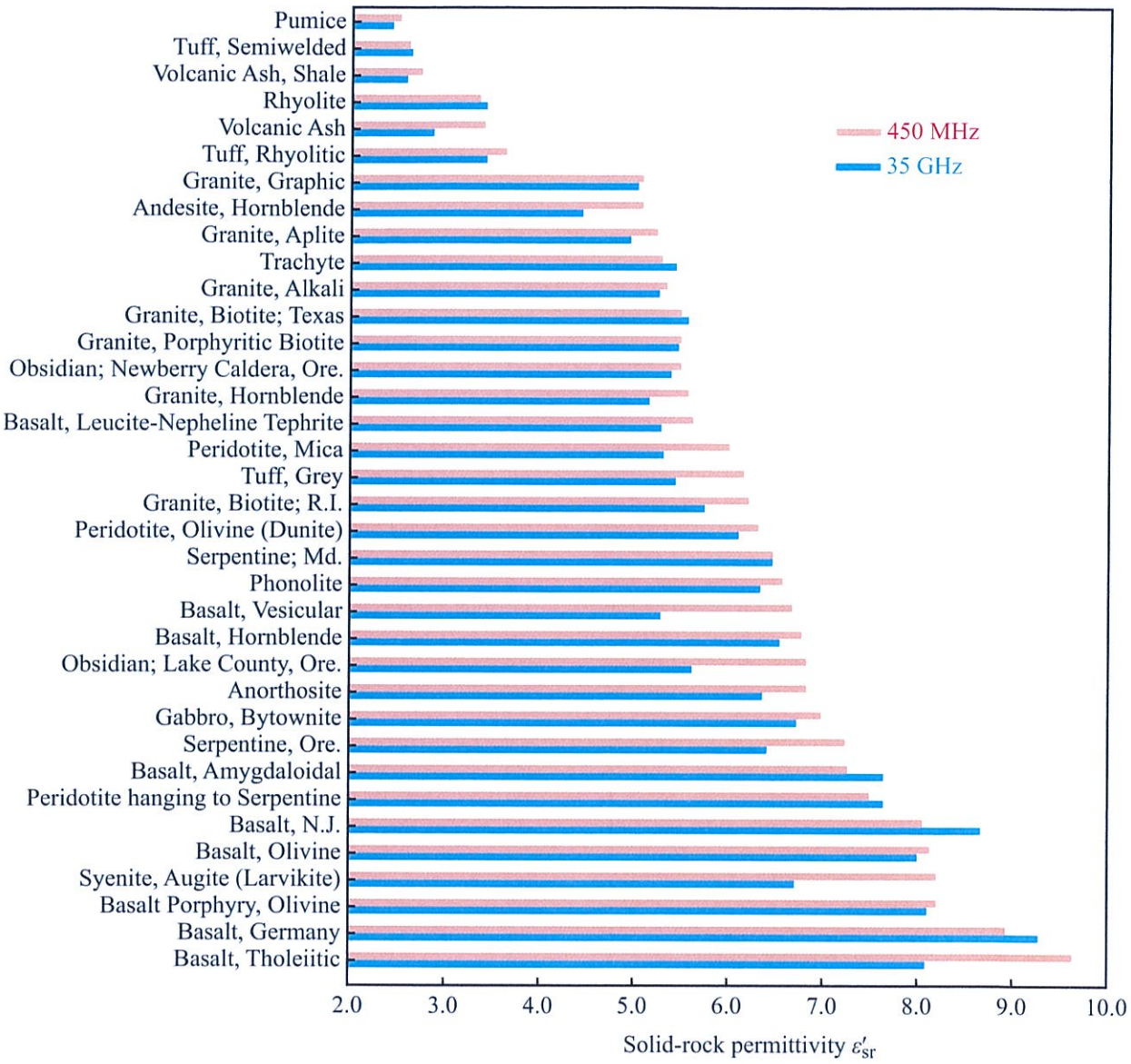

Figure 4-25: A comparison of the permittivities of solid rocks at 450 MHz and 35 GHz [from Campbell and Ulrichs, 1969].

4-7.2 Solid Rocks

According to the data shown in Fig. 4-25, among 36 types of solid rocks, ε'_{sr} varies between 2.5 and 9.6, and the values measured at 450 MHz are not statistically different from those measured at 35 GHz, suggesting that ε'_{sr} is frequency-independent in the microwave band. This conclusion is supported by the spectra shown in Fig. 4-26 for four typical examples of the 80 rock types examined by Ulaby et al. (1990a). Dielectric measurements made as a function of temperature revealed that ε'_{sr} is temperature-independent also.

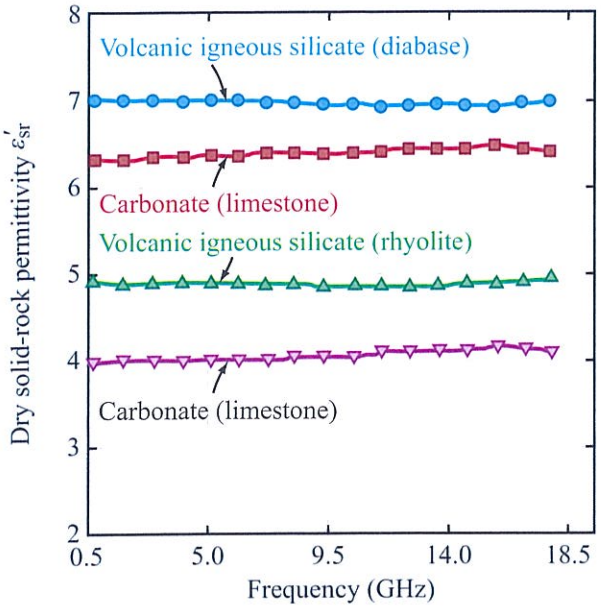

Figure 4-26: Typical examples of measured permittivity spectra [Ulaby et al., 1990a].

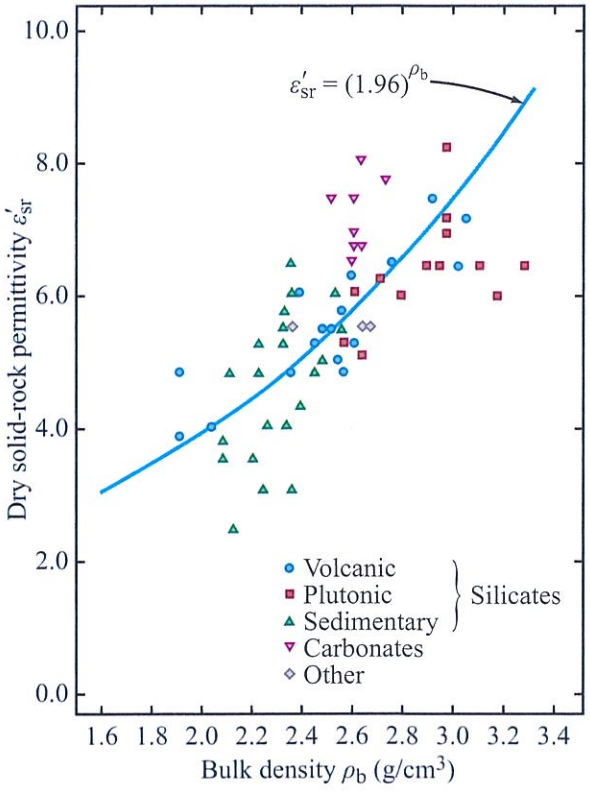

Figure 4-27: Variation of ε'_{sr} with rock bulk density [Ulaby et al., 1990a].

The variation of ε'_{sr} with bulk density ρ_b is displayed in Fig. 4-27. The figure includes measured data as well as an empirical fit given by

$$\varepsilon'_{sr} = (\varepsilon'_p)^{\rho_b} = 2^{\rho_b}, \tag{4.62}$$

where $\varepsilon'_p = 2$ is the average permittivity of powdered rocks. The deviation from a smooth variation with ρ_b is attributed to differences in mineralogy among the various types of rocks.

Unlike the frequency-independent behavior of ε'_{sr}, the loss factor ε''_{sr} exhibits a definite variation with frequency for all rocks tested by Ulaby et al. (1990a). Typical examples are shown in Fig. 4-28. The frequency variation of ε''_{sr} is attributed, at least in part, to the dispersion spectrum of bound water within the rock samples.

Analysis of the measured data of ε''_{sr} led to the following conclusions:

(a) No apparent correlation between ε''_{sr} and bulk density ρ_b.

(b) At 1.6 GHz, the range of ε''_{sr} among the 80 different types of rocks extended between 0.002 and 0.24, and the corresponding range at 16 GHz extended between 0.002 and 0.18. Similar ranges of values were reported by Vaccaneo et al. (2004) at L-band.

(c) Most rock types exhibited a frequency variation of the form

$$\varepsilon''_{sr} = a + \frac{b}{f}, \tag{4.63}$$

where a and b are constants specific to the rock type under consideration and f is frequency. No apparent correlation could be established between coefficients a and b and bulk density ρ_b.

In summary, for individual rock types, ε''_{sr} exhibits a predictable variation similar to that of the plots shown in

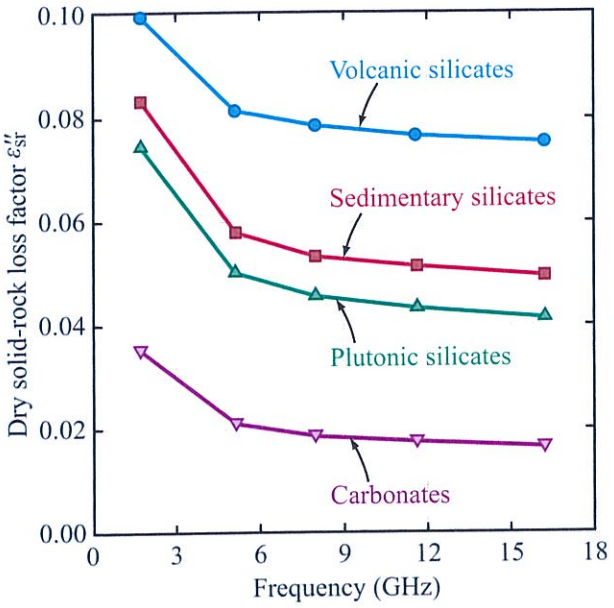

Figure 4-28: Variation of ε''_{sr} with frequency for four types of rocks [Ulaby et al., 1990a].

Fig. 4-28, but the magnitude of ε''_{sr} does not appear to be related to bulk density.

4-8 Dielectric Constant of Soils

4-8.1 Dry Soil

In the absence of liquid water, the microwave dielectric constant of soil, ε_{soil}, is essentially independent of both temperature and frequency. Moreover, $2 \lesssim \varepsilon'_{soil} \lesssim 4$ and $\varepsilon''_{soil} < 0.05$. Based on experimental measurements of several soil types, Dobson et al. (1985) determined that ε'_{soil} can be modeled as

$$\varepsilon'_{soil} = (1 + 0.44\rho_b)^2 \qquad \textbf{(dry soil)}, \qquad (4.64)$$

where ρ_b is the soil bulk density.

4-8.2 Wet Soil

A wet-soil medium is a mixture of soil particles, air pockets, and liquid water. The water contained in the soil usually is divided into two fractions: (a) ***bound water***, and (b) ***free water***. Bound water refers to water molecules that are contained in the first few molecular layers surrounding the soil particles and therefore are tightly held by the soil particles due to the influence of matric and osmotic forces. Because the matric forces acting on a water molecule decrease rapidly with increasing distance from the soil particle, water molecules that are located several molecular layers away from soil particles are able to move within the soil medium with relative ease, and hence are referred to as "free."

Dividing the water into bound and free fractions is only an approximate description of the actual distribution of water molecules in the soil medium and is based on a somewhat arbitrary criterion for establishing the transition point between bound and free water layers. The amount of water contained in the molecular layer adjoining the soil particles is directly proportional to the total surface area of the soil particles contained in a unit volume. The total surface area of the particles is, in turn, a function of the size distribution and mineralogy of the soil particles. For the most part, a soil is assigned to a ***textural class*** on the basis of its ***particle-size distribution***.

Soil particles are classified as sand, silt, or clay, according to size (Fig. 4-29). Because all soils contain a distribution of particle sizes, it is convenient to classify a soil by the weight-percent of the soil within each specific size category (sand, silt, or clay). The relative percentages of the three size categories then determine the soil's textural class (Fig. 4-30 shows the U.S. Department of Agriculture triaxial classification system). Soil type refers to a subdivision of one of the soil textural classes shown in Fig. 4-30.

The two terms commonly used to characterize the moisture content of a soil sample are ***volumetric***

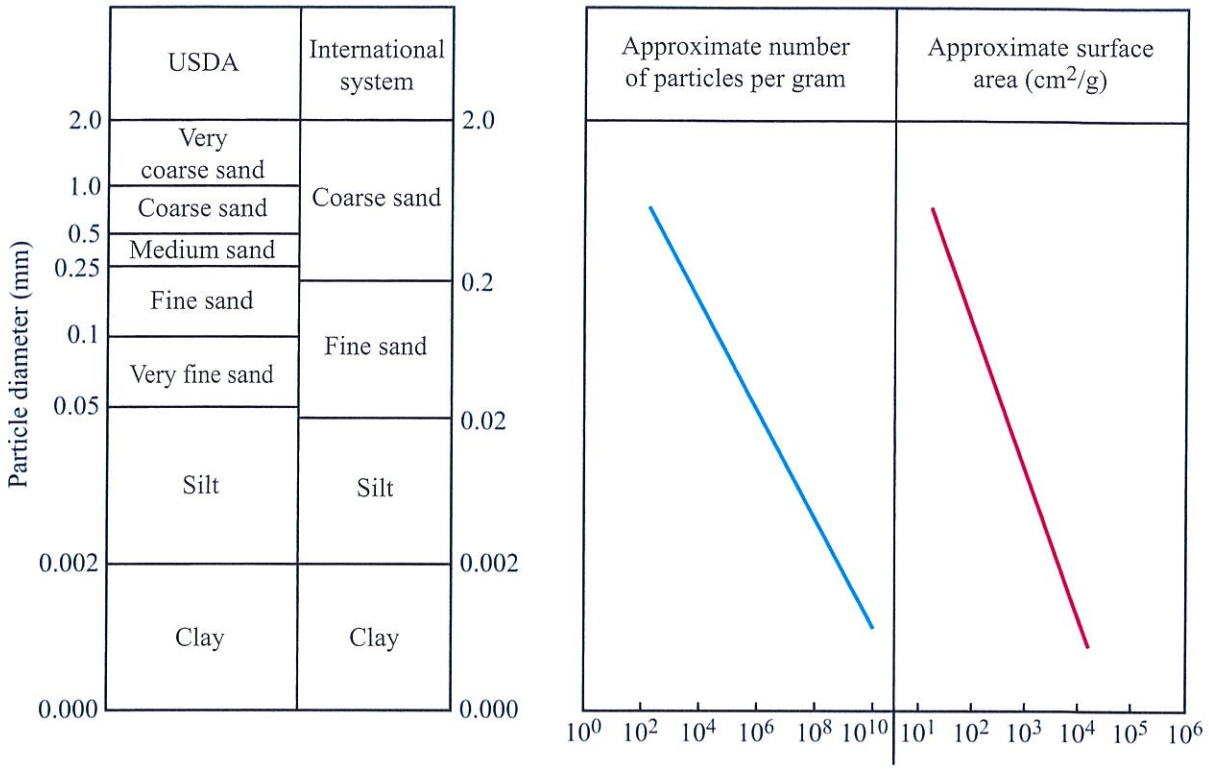

Figure 4-29: Particle-size classes, number of particles, and external surface area based on spherical particles of density 2.65 g/cm^3 [modified from Birkeland, 1974].

moisture m_v and ***gravimetric moisture*** m_g,

$$m_v = \frac{V_w}{V_t} = \frac{V_w}{V_{dry}} = \frac{W_w \rho_b}{W_{dry} \rho_w} = \frac{W_w \rho_b}{W_{dry}} \text{ cm}^3/\text{cm}^3 \text{ or g/cm}^3, \tag{4.65a}$$

and

$$m_g = \frac{W_w}{W_{dry}} \times 100 = 100 \frac{m_v}{\rho_b} \text{ (\%)}, \tag{4.65b}$$

where W_w and W_{dry} are the weights of the water in the sample and of the dry sample, respectively; V_w is the water volume; V_t is the total volume of the sample, which includes the volumes of air, soil, and water and is equal to the volume of the dry sample (assuming that when water is added to the sample, it fills air pockets but does not increase the total volume); ρ_b is the bulk density of the dry soil sample; and $\rho_w = 1$ g/cm^3 is the density of water. Although m_v, being a fraction, is unitless, it usually is expressed in cm^3/cm^3 or g/cm^3.

In general, a soil medium is electromagnetically a four-component dielectric mixture consisting of air, bulk soil, bound water, and free water. Due to the intensity of the forces acting upon it, a bound water molecule interacts with an incident electromagnetic wave in much the same way that it does when it is in the form of ice, thereby exhibiting a dielectric dispersion spectrum that is very different from that of free water. The complex dielectric constants of bound and free water are functions of the electromagnetic frequency f, the physical temperature T, and the salinity S. Hence, the dielectric constant of the soil mixture is, in general, a function of (a) f, T, and S, (b) the total volumetric

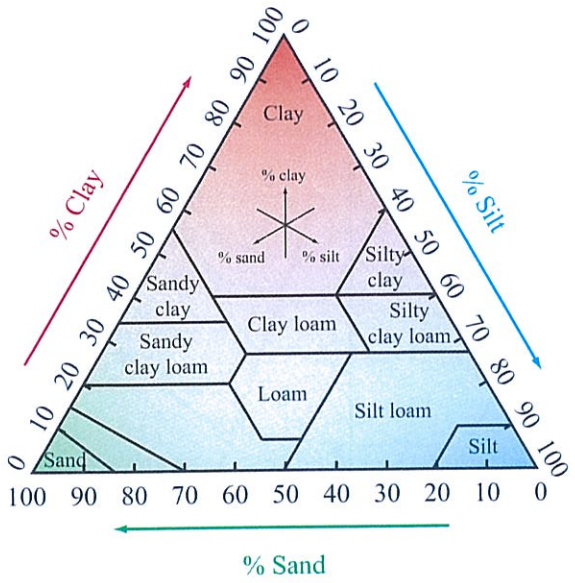

Figure 4-30: Soil textured classification triangle.

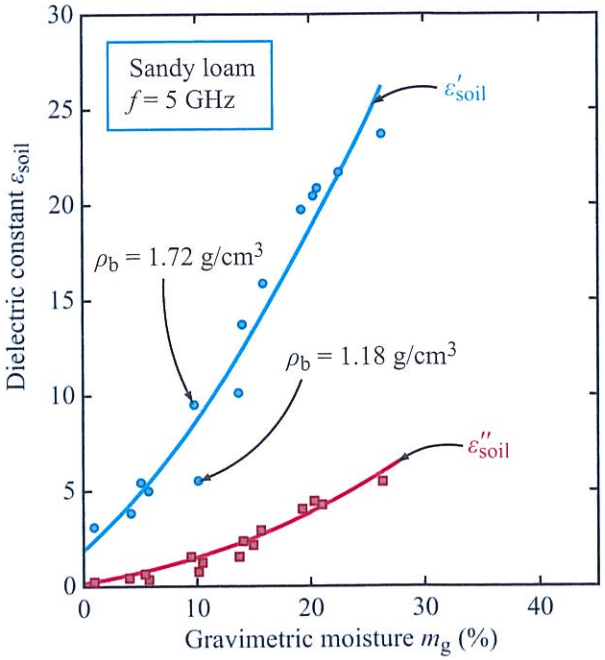

(a) ε_{soil} versus gravimetric moisture

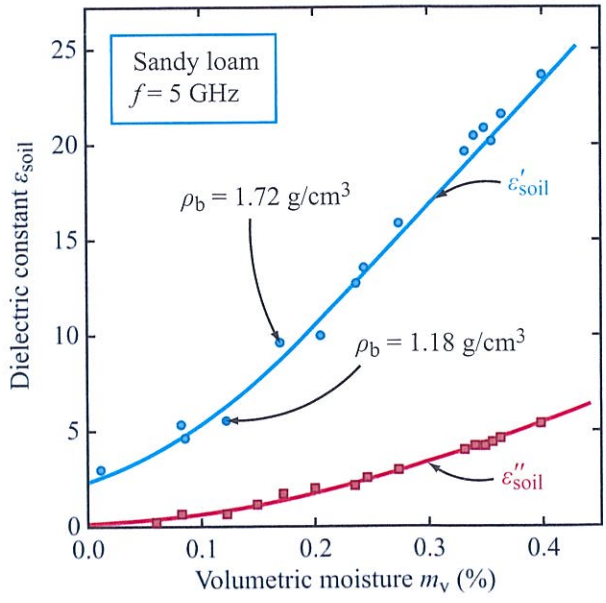

(b) ε_{soil} versus volumetric moisture

Figure 4-31: Comparison of measured soil dielectric constant data plotted as a function of (a) gravimetric moisture content and (b) volumetric moisture content [from Hallikainen et al., 1985].

water content m_v, (c) the relative fractions of bound and free water, which are related to the particle-size distribution (or soil texture), (d) the bulk soil density ρ_b, (e) the shape of the soil particles, and (f) the shape of the water inclusions. We will endeavor to describe ε_{soil} by a relatively straightforward model that accounts for most of the dependence on this long list of variables.

Numerous studies have been conducted to determine the dielectric behavior of soil-water mixtures, most notably those reported by Wang et al. (1980), Dobson et al. (1985), Hallikainen et al. (1985), Roth et al. (1990), and Peplinski et al. (1995). The measured dielectric data usually are plotted as a function of either m_v or m_g, and occasionally, of both.

From the standpoint of dielectric mixing models, the volumetric measure is preferred because the dielectric constant of the soil-water mixture is a function of the water volume-fraction in the mixture. This preference is demonstrated by Fig. 4-31, in which a greater degree of scattering about the regression curve is apparent for the plots of ε'_{soil} and ε''_{soil} versus m_g [Fig. 4-31(a)] than for those plotted versus m_v [Fig. 4-31(b)]. Additionally, measurements made for two soil samples

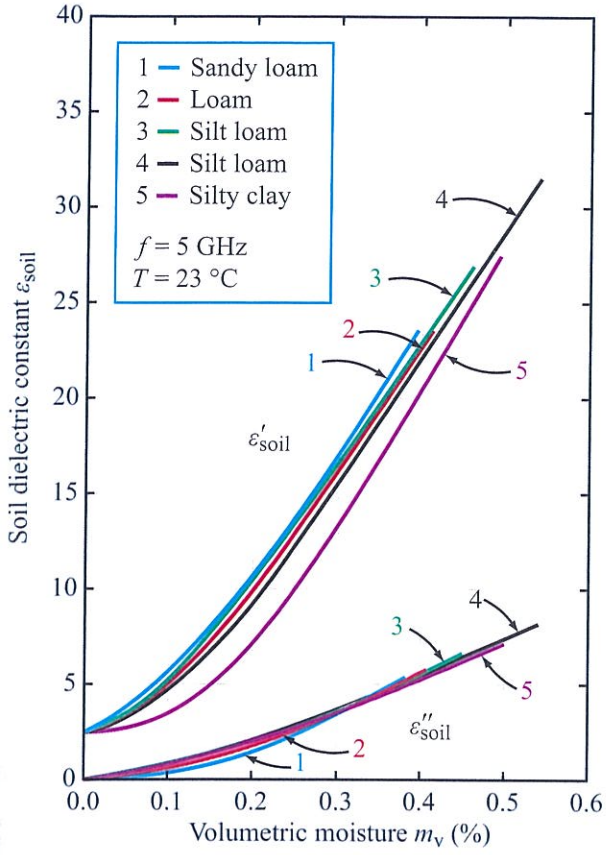

Figure 4-32: Measured dielectric constant for five soils at 5 GHz [Hallikainen et al., 1985].

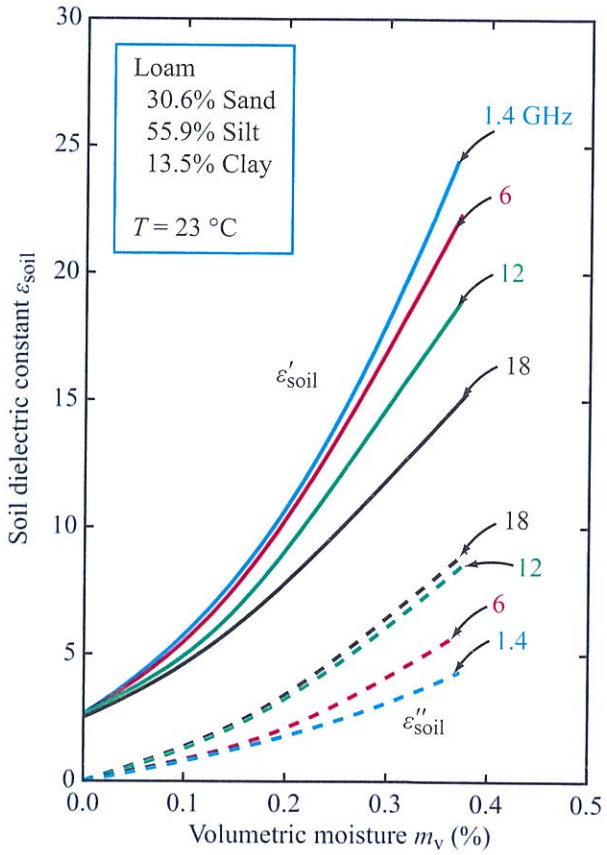

Figure 4-33: Measured dielectric constant as a function of volumetric moisture content for a loamy soil at four microwave frequencies [Hallikainen et al., 1985].

with approximately the same m_g, but significantly different bulk densities, resulted in significantly different values for ε_{soil}. However, samples with the same m_v but different bulk densities resulted in dielectric values that were approximately the same for both samples.

The curves shown in Fig. 4-32 depict the measured variation of ε_{soil} with m_v for five soil types at 5 GHz. Similar responses were measured at other frequencies between 1.4 and 18 GHz. The indicated moisture range for each soil type extends between $m_v = 0$ and the highest moisture content that can be supported by that soil type without producing drainage.

Figure 4-33 illustrates the role of frequency for one of the soil types measured by Hallikainen et al. (1985), which indicates that ε'_{soil} decreases with increasing frequency between 1.4 and 18 GHz, whereas ε''_{soil} increases with increasing frequency. The character of the frequency response of ε_{soil} is similar to that of water (Section 4-1). The dependence of ε_{soil} on frequency is more clearly displayed in Fig. 4-34, which shows the spectra for ε'_{soil} and ε''_{soil} for several values of m_v.

The dependence of ε_{soil} on temperature was examined by Hoekstra and Delaney (1974) at 10 GHz and by Hallikainen et al. (1984b) over a wide frequency range extending from 3 GHz to 37 GHz. Above 0 °C, ε'_{soil} and ε''_{soil} are weakly dependent on temperature, but as T crosses the freezing temperature of water, both ε'_{soil}

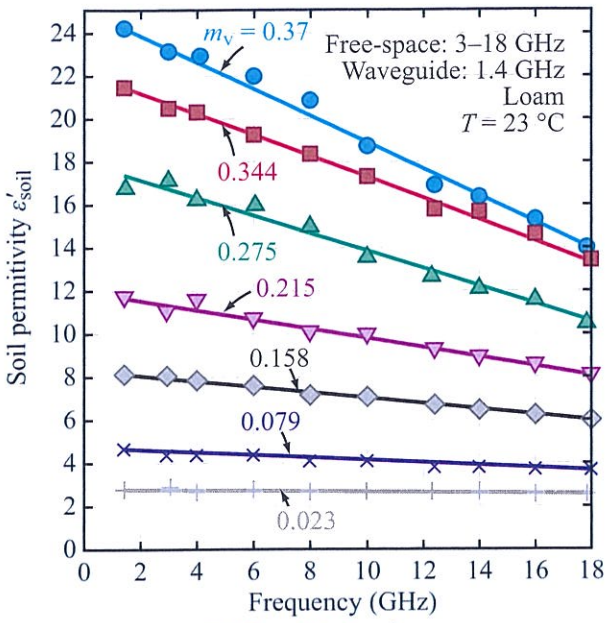

(a) Permittivity ε'_{soil}

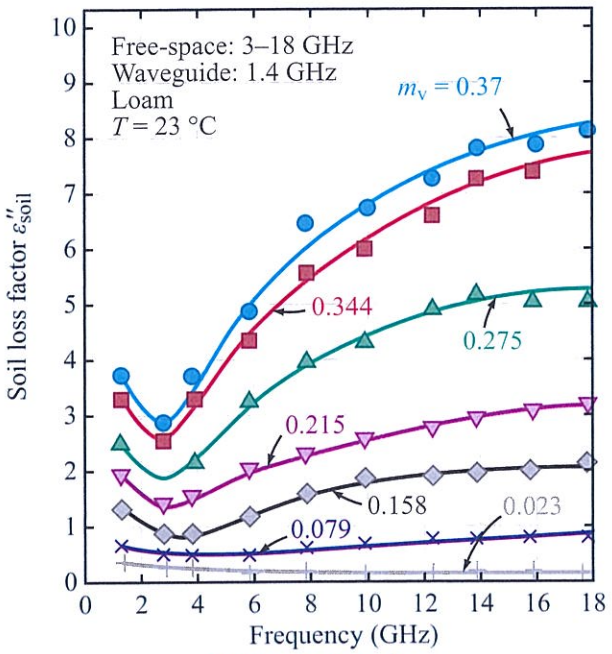

(b) Loss factor ε''_{soil}

Figure 4-34: Measured (a) permittivity and (b) loss factor of loamy soil as a function of frequency with volumetric moisture content as a parameter [Hallikainen et al., 1985].

and ε''_{soil} change markedly, as illustrated by the data in Fig. 4-35.

To model the dielectric behavior of soils at microwave frequencies, Dobson et al. (1985) used a four-component model consisting of solid soil material, air, bound water, and free water. Using a refractive-like model along the lines of Eq. (4.45), together with representative values for the density of solid soil material, they developed the following semiempirical model for ε_{soil}:†

$$\varepsilon'_{soil} = [1 + 0.66\rho_b + m_v^{\beta_1}(\varepsilon'_w)^{\alpha} - m_v]^{1/\alpha}, \tag{4.66a}$$

$$\varepsilon''_{soil} = m_v^{\beta_2}\varepsilon''_w, \tag{4.66b}$$

where ρ_b is the bulk density of the soil in g/cm^3 (if the value of ρ_b is unknown, it is recommended that the typical value of 1.7 g/cm^3 be used), m_v is the volumetric moisture content in g/cm^3, and ε_w is the dielectric constant of water. In the model, ε_w is given by the single Debye model of Section 4-1, with an added conductivity term for ε''_w. That is,

$$\varepsilon'_w = \varepsilon_{w\infty} + \frac{\varepsilon_{w0} - \varepsilon_{w\infty}}{1 + (2\pi f\tau_w)^2}, \tag{4.67a}$$

$$\varepsilon''_w = \frac{2\pi f\tau_w(\varepsilon_{w0} - \varepsilon_{w\infty})}{1 + (2\pi f\tau_w)^2} + \left(\frac{2.65 - \rho_b}{2.65m_v}\right)\frac{\sigma}{2\pi\varepsilon_0 f}. \tag{4.67b}$$

The expressions for ε_{w0}, $\varepsilon_{w\infty}$, and τ_w are given in Section 4-1, and $\varepsilon_0 = 8.854 \times 10^{-12}$ F/m. The exponents α, β_1, and β_2, and the effective conductivity σ are related to the soil properties. Their empirically determined expressions are:

$$\alpha = 0.65 \tag{4.68a}$$

$$\beta_1 = 1.27 - 0.519S - 0.152C, \tag{4.68b}$$

$$\beta_2 = 2.06 - 0.928S - 0.255C, \tag{4.68c}$$

$$\sigma = -1.645 + 1.939\rho_b - 2.256S + 1.594C, \tag{4.68d}$$

where S and C represent the mass fractions of sand and clay, respectively (i.e., $0 \le S \le 1$ and the same range applies to C).

† **Computer Code 4.7.**

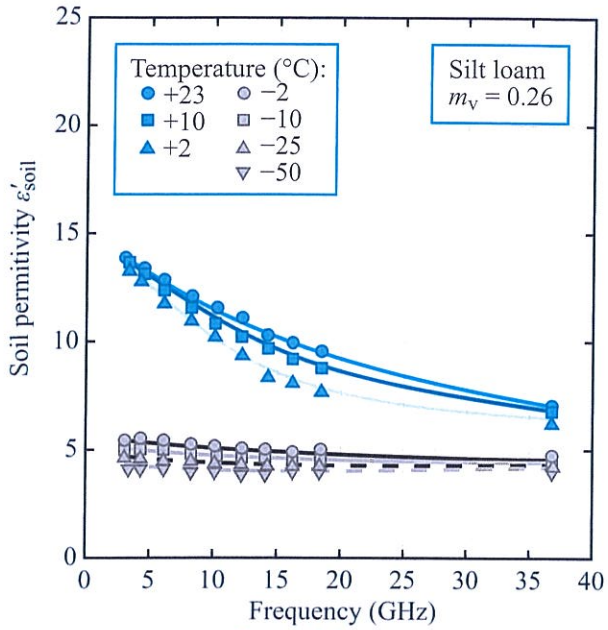

(a) Permittivity ε'_{soil}

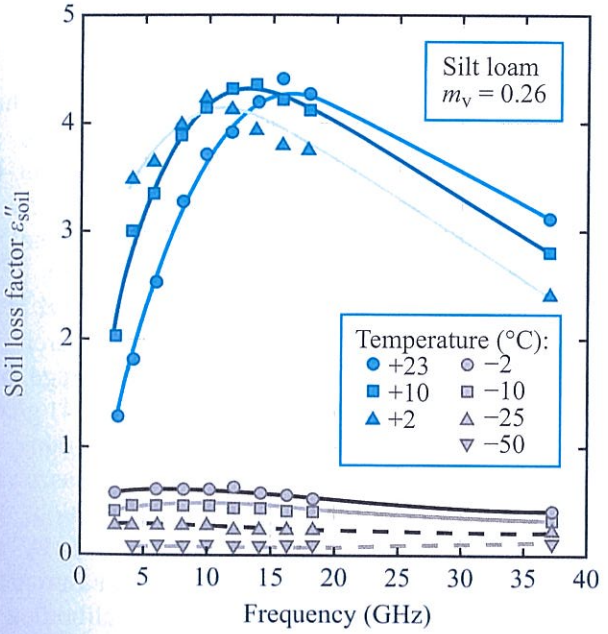

(b) Loss factor ε''_{soil}

Figure 4-35: Measured permittivity and loss factor of silt loam soil as a function of frequency with temperature as a parameter [from Hallikainen et al., 1984b].

For the 809 measurements of ε'_{soil}—and the same number for ε''_{soil}—covering five soil types, multiple frequencies between 1.4 and 18 GHz, and numerous moisture conditions, the multiple correlation coefficient between the measured values of ε_{soil} and the model-calculated values was reported to be $R^2 = 0.98$ for ε'_{soil} and 0.99 for ε''_{soil}.

When applying the model given by Eq. (4.66), we can either use the detailed expressions for ε_w of free water given in Section 4-1 or avail ourselves of the simplified version specific to $T = 23$ °C and $\rho_b = 1.7$ g/cm^3:

$$\varepsilon'_w = 4.9 + \frac{74.1}{1+(f/f_0)^2}, \tag{4.69a}$$

$$\varepsilon''_w = \frac{74.1(f/f_0)}{1+(f/f_0)^2} + 6.46\,\frac{\sigma}{f}, \tag{4.69b}$$

with f and f_0 expressed in GHz and $f_0 = 18.64$ GHz (which is the relaxation frequency of water at 23 °C).

According to the report by Dobson et al. (1985), the proposed model provided excellent overall agreement with the dielectric data measured across most of the 1.4–18 GHz range, but the fit was not as good at 1.4 GHz.

4-8.3 ε_{soil} in 0.3–1.5 GHz Band

Peplinski et al. (1995) conducted a study of several soil types, with specific focus on the dielectric behavior in the 0.3–1.3 GHz range. An example of their results is shown in Fig. 4-36, in which measured data are compared with a modified version of the model given by Eqs. (4.67) and (4.68). The modification involves the expression for the conductivity σ. Instead of Eq. (4.68d), they proposed the empirically determined expression

$$\sigma = 0.0467 + 0.22\rho_b - 0.411S + 0.661C. \tag{4.70}$$

(0.3–1.3 GHz)

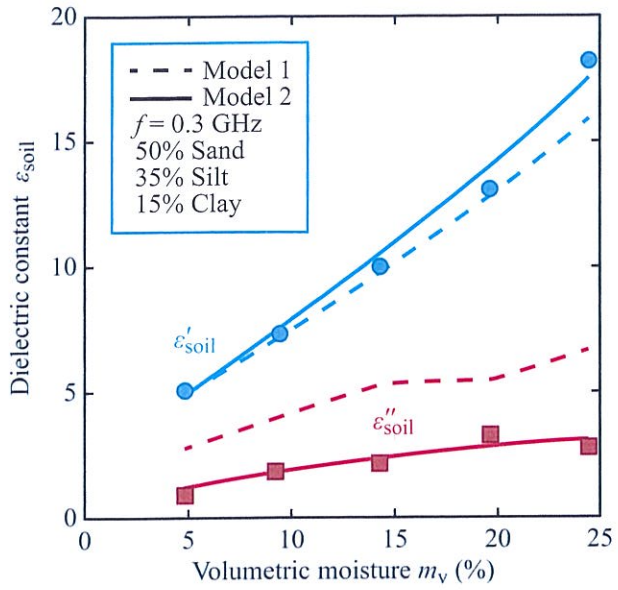

(a) ε_{soil} at 0.3 GHz

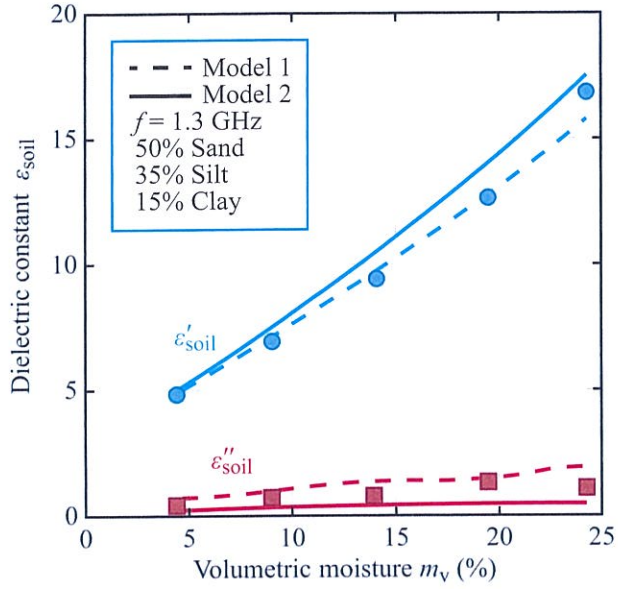

(b) ε_{soil} at 1.3 GHz

Figure 4-36: Comparison of values of ε' and ε'' measured at 0.3 and 1.3 GHz with calculations based on Model 1 given by Eqs. (7.67) to (7.69) and Model 2 with the corrections given by Eq. (4.70) [Peplinski et al., 1995].

4-9 Dielectric Constant of Vegetation

From the standpoint of wave propagation, a vegetation canopy is a dielectric mixture consisting of discrete dielectric inclusions (such as leaves, stalks, and fruit) distributed in a host material (air). In most canopies, the sizes of the inclusions are either comparable to or larger than the wavelength in the microwave region, which means that the canopy is an inhomogeneous, anisotropic medium. Propagation through such a medium entails both absorption and scattering.

Models describing the scattering and emission behavior of a vegetation canopy often are developed in terms of the volume absorption and scattering coefficients of the canopy, κ_a and κ_s. In general, both quantities are governed by the dielectric constant, volume fraction, and geometry (i.e., the shape and orientation relative to the EM wave's electric field) of the various types of inclusions present in the canopy.

4-9.1 Dielectric Constant of Canopy Constituents

Dielectric measurements of several grain types have been reported over a wide range of frequencies. In the case of winter wheat, the dielectric constant has been measured over the range extending from 250 Hz in the audio frequency band to 12.2 GHz in the microwave band (Nelson and Stetson, 1976). An example illustrating the moisture dependence of ε_v at 1.0 and 12.2 GHz is shown in Fig. 4-37. The measurements were made for wheat heads having an average bulk density of 0.76 g/cm^3 and a kernel density of 1.41 g/cm^3. These and similar measurements for other grains and seeds (Nelson, 1973, 1976, 1978, 1979; Kraszewski, 1978) all share a common fundamental limitation: they rarely exceed moisture levels of 25 percent by wet weight. In most cases, the purpose of the measurements was to support the development and calibration of moisture meters for the grain industry. Hence, the moisture range-of-interest was usually below 25 percent, which is lower than the typical moisture content of the grain at harvest. From the standpoint of remote sensing, the range of interest for moisture content is between 40 percent and 90 percent by wet weight. Although the

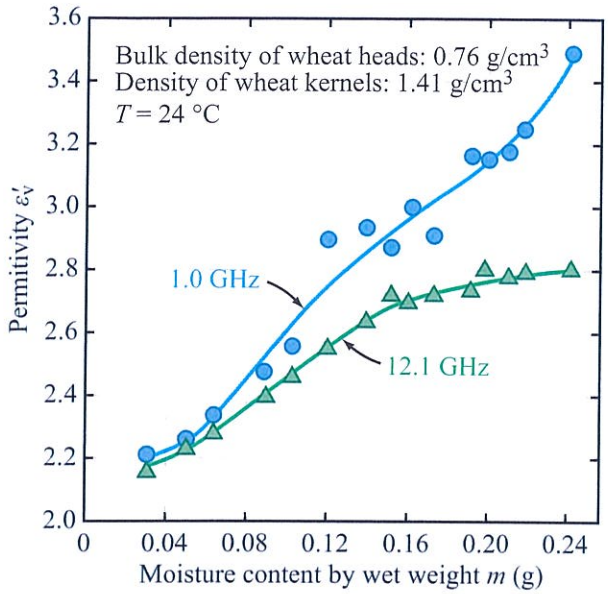

(a) Permitivity ε'_v

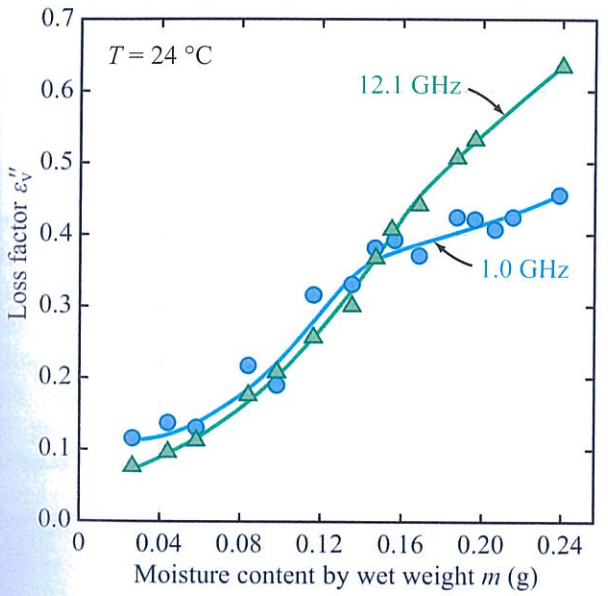

(b) Loss factor ε''_v

Figure 4-37: Measured dielectric constant of red winter wheat heads as a function of moisture content [from Nelson and Stetson, 1976].

available dielectric data for grains and seeds may not be directly applicable to remote-sensing problems, they can nonetheless supplement higher moisture data.

The moisture content of a vegetation material, such as leaves or stalks, is measured on a ***gravimetric*** wet-weight basis (m_g) or on a ***volume basis*** (m_v). The two quantities are related by

$$m_g = \frac{m_v}{m_v + (1 - m_v)\rho_s}, \tag{4.71a}$$

$$m_v = \frac{\rho_s m_g}{1 - m_g(1 - \rho_s)}, \tag{4.71b}$$

where ρ_s is the dry density of the solid material. A typical value of ρ_s for leaves is 0.3 g/cm^3. The range of m_g extends from 0 to about 0.9, and the corresponding range of m_v is 0 to 0.7 (for $\rho_s \approx 0.3$).

Using a waveguide transmission technique, Ulaby and Jedlicka (1984) measured the dielectric properties of leaves and stalks of corn and wheat over the 1.1 to 8.4 GHz range. Examples are shown in Fig. 4-38 for corn leaves at three microwave frequencies. As discussed shortly, among the important parameters governing the behavior of ε'_v and ε''_v is the salinity S of the fluid samples extracted from the vegetation material. Figure 4-38 displays dielectric data measured for corn leaves with $S = 11$ psu.

In a follow-up study, dielectric measurements were conducted over the 0.2 to 20 GHz range for various types of vegetation material (El-Rayes and Ulaby, 1987; Ulaby and El-Rayes, 1987). An example illustrating the spectra of ε'_v and ε''_v at various moisture levels is shown in Fig. 4-39. The data were used in the development of the dielectric model introduced in Section 4-9.2. Data measured for corn stalks and other types of vegetation were found to exhibit a moisture dependence very similar to that for corn leaves.

Pressure techniques were used to extract samples of the fluids contained in some of the vegetation material, so as to measure the dielectric spectrum of the fluid. Figure 4-40 displays the measured spectrum for the fluid contained in a freshly cut corn stalk. Also shown in the figure is the dielectric spectrum computed for saline water with a salinity of 7 psu, which was the measured salinity of the extracted fluid. The measured and calculated spectra are in very close agreement.

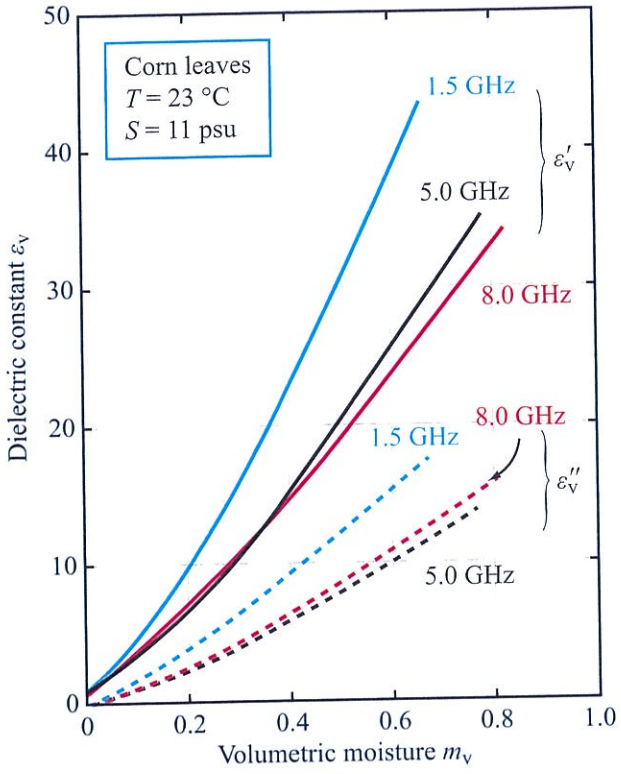

Figure 4-38: Measured moisture dependence of the dielectric constant of corn leaves at 1.5, 5.0, 8.0 GHz [Ulaby and Jedlicka, 1984].

The role of temperature was examined by measuring the dielectric constant as the temperature was slowly lowered from room temperature at 22 °C down to −32 °C. At a salinity of 5 psu, the freezing temperature of the vegetation fluid should be around −0.3 °C. Hence, the expectation was that the water in the corn leaves would freeze when the temperature reached between 0 and −1 °C. The results shown in Fig. 4-41 suggest otherwise; the fluid in the corn leaf goes through a supercooling state down to about −6 °C, and then it freezes instantaneously.

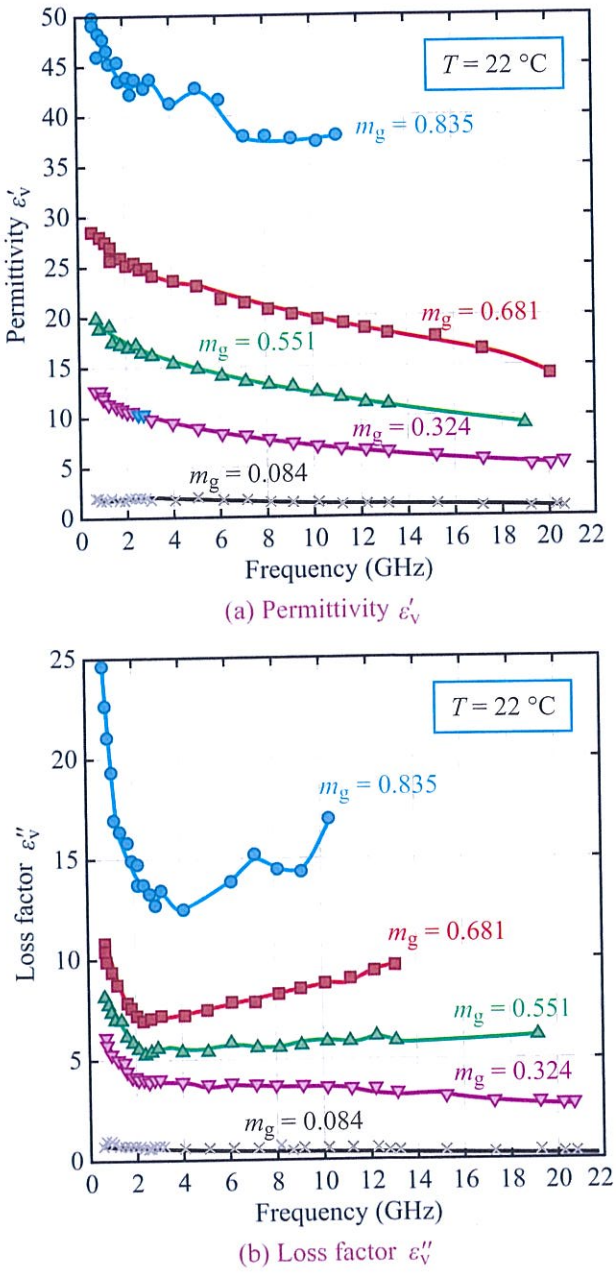

(a) Permittivity ε'_v

(b) Loss factor ε''_v

Figure 4-39: Family of dielectric spectra for corn leaves at $T = 22$ °C and various moisture contents [El-Rayes and Ulaby, 1987].

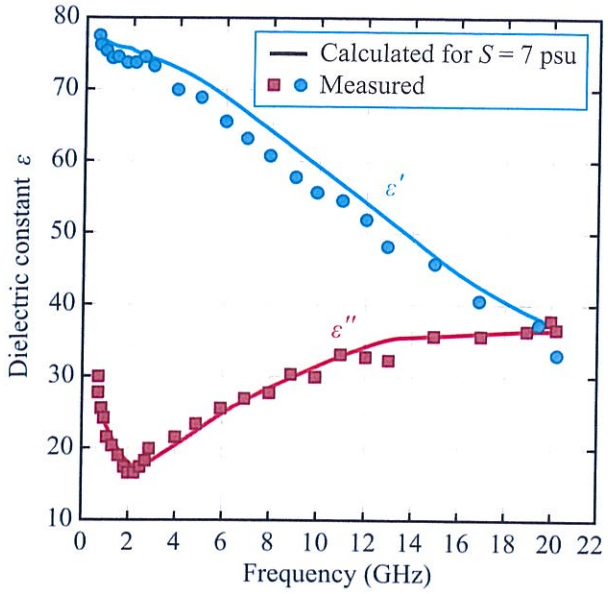

Figure 4-40: Measured and calculated dielectric spectra of the fluid extracted from corn stalks [El-Rayes and Ulaby, 1987].

4-9.2 Dielectric Model

In most dielectric models of a solid material containing water (Section 4-4), the mixture is treated as an inhomogeneous medium consisting of discrete water particles dispersed in the bulk material (as host). The water particles are assigned a shape (such as spherical or cylindrical) in order to match the model to experimental data. Such models are unrealistic for vegetation because the water inside a leaf is closer to being spatially continuous than discrete. Accordingly, Ulaby and El-Rayes (1987) introduced a linear model for the dielectric constant of vegetation in the form of an additive mixture of three components:†

$$\varepsilon_v = \varepsilon_r + v_{fw}\varepsilon_w + v_{bw}\varepsilon_b, \qquad (4.72)$$

where ε_r is a nondispersive ***residual component*** to be determined empirically, ε_w and ε_b are the complex dielectric constants of ***free water*** and ***bound water***,

†Computer Code 4.8.

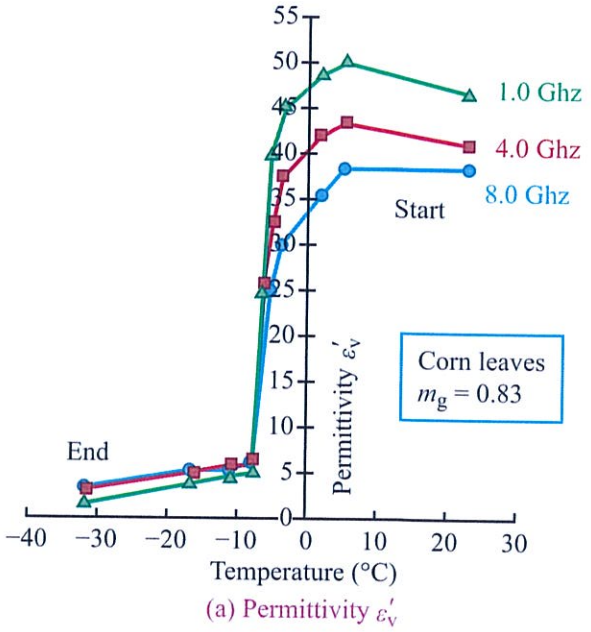

(a) Permittivity ε'_v

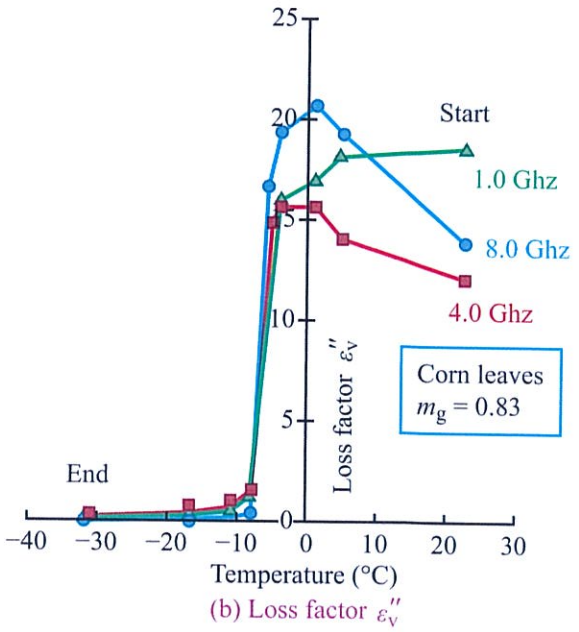

(b) Loss factor ε''_v

Figure 4-41: Variation of ε_r of corn leaves with decreasing temperature from 22 °C down to −32 °C [El-Rayes and Ulaby, 1987].

respectively, and v_{fw} and v_{bw} are their associated volume fractions. The real and imaginary parts of ε_v are

$$\varepsilon'_v = \varepsilon_r + v_{fw}\varepsilon'_w + v_{bw}\varepsilon'_b, \tag{4.73a}$$

$$\varepsilon''_v = v_{fw}\varepsilon''_w + v_{bw}\varepsilon''_b. \tag{4.73b}$$

Free water

For the free-water component, the expressions for ε'_w and ε''_w given by Eqs. (4.14a) and (4.14b) are quite adequate, but because the free water in vegetation includes low concentrations of salts and sugars (salinity S seldom exceeds 15 psu), the expression for ε''_w requires the addition of a conductivity term. That is,

$$\varepsilon'_w = \varepsilon_{w\infty} + \frac{\varepsilon_{w0} - \varepsilon_{w\infty}}{1 + (f/f_0)^2} \tag{4.74a}$$

$$\varepsilon''_w = \frac{(f/f_0)(\varepsilon_{w0} - \varepsilon_{w\infty})}{1 + (f/f_0)^2} + \frac{\sigma_i}{2\pi\varepsilon_0 f}, \tag{4.74b}$$

where f_0 is the relaxation frequency of free water. The ionic conductivity σ_i is a function of the salinity S and the temperature T, and its functional form is given by Eq. (4.21f). At $T = 22$ °C, the relaxation frequency of water is 18 GHz, and the expressions for ε'_w and ε''_w become

$$\varepsilon'_w = 4.9 + \frac{74.4}{1 + (f/18)^2}, \tag{4.75a}$$

$$\varepsilon''_w = \frac{74.4(f/18)}{1 + (f/18)^2} + \frac{18\sigma_i}{f}, \tag{4.75b}$$

where f is in GHz and

$$\sigma_i \approx 0.17S - 0.0013S^2 \quad \text{(S/m)}. \tag{4.75c}$$

Bound water

A water molecule is considered to be in the "bound" state if its response to a suddenly applied electric field is inhibited because of some force acting on it. When in the bound state, the relaxation time τ of a water molecule is longer than when in the free state, but it is difficult to quantitatively relate the type of force and its magnitude to the increase in τ. To develop a model for the dielectric constant of the bound-water component in the vegetation mixture, Ulaby and El-Rayes (1987) conducted dielectric measurements for sucrose-water mixtures. Sucrose was chosen because it is a good example of the organic substances present in vegetation, and the binding arrangement of sucrose-water molecules is well known, thereby allowing them to compute the bound water concentration. Dielectric measurements conducted from 0.2 to 20 GHz for a sucrose-water solution at room temperature (22 °C) were fitted to a Cole-Cole dispersion equation of the form

$$\varepsilon'_b - j\varepsilon''_b = 2.9 + \frac{55}{1 + (jf/0.18)^{0.5}}. \tag{4.76}$$

The factor 0.18 represents the relaxation frequency of bound water in GHz, which is exactly two orders of magnitude smaller than that for free water. In a Cole-Cole equation, the exponent of (f/f_0) may be smaller than 1. In the present case, the value 0.5 was found to provide an optimum fit to the measured data, as demonstrated by Fig. 4-42. Rationalizing Eq. (4.76) leads to

$$\varepsilon'_b = 2.9 + \frac{55(1 + \sqrt{f/0.36})}{(1 + \sqrt{f/0.36})^2 + (f/0.36)}, \tag{4.77a}$$

$$\varepsilon''_b = + \frac{55\sqrt{f/0.36}}{(1 + \sqrt{f/0.36})^2 + (f/0.36)}, \tag{4.77b}$$

with f in GHz.

Empirical fits

By fitting the measured dielectric data to the dielectric model, the remaining quantities in Eq. (4.73) were found to assume the forms

$$\varepsilon_r = 1.7 - 0.74m_g + 6.16m_g^2, \tag{4.78a}$$

$$v_{fw} = m_g(0.55m_g - 0.076), \tag{4.78b}$$

$$v_{bw} = \frac{4.64m_g^2}{1 + 7.36m_g^2}. \tag{4.78c}$$

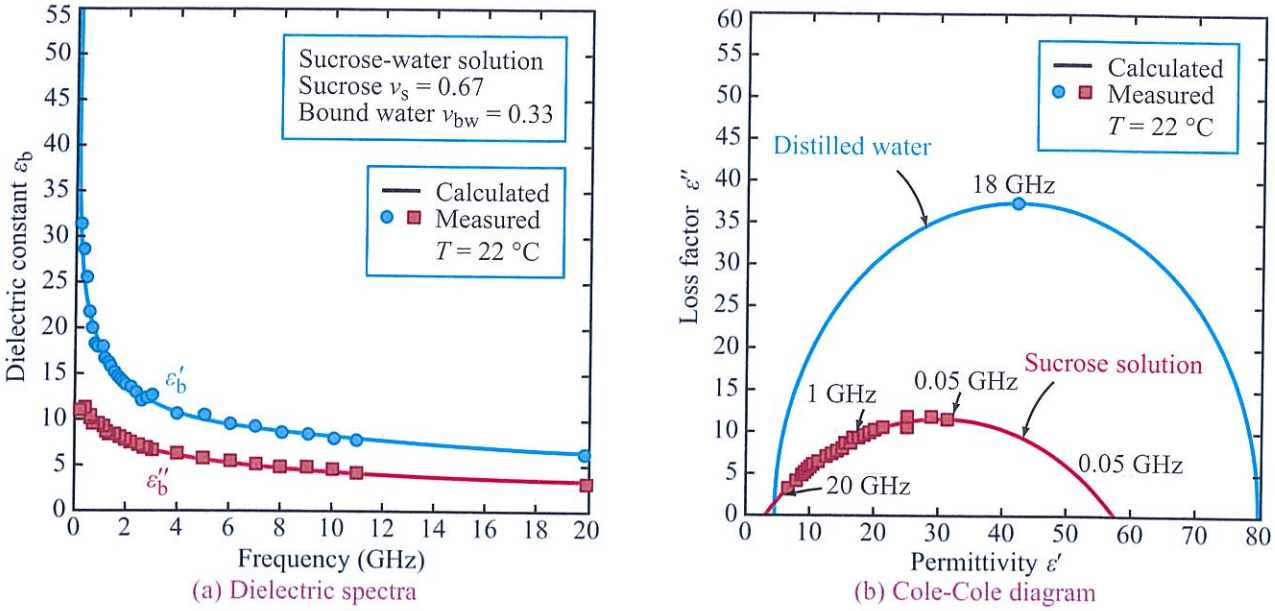

Figure 4-42: (a) Measured dielectric spectrum of sucrose-water solution and theoretical spectrum calculated according to Eq. (4.76). (b) Cole-Cole diagrams for distilled water and sucrose solution.

The residual dielectric constant ε_r varies from 1.7 for dry vegetation to 4.5 for $m_g = 0.7$. Since it represents the bulk vegetation material, it should not depend on m_g, but including a dependence on m_g leads to a better fit. Examples illustrating the dielectric spectra of corn leaves are shown in Fig. 4-43, and the variation of ε_v with m_g is displayed in Fig. 4-44. Even though the model was developed on the basis of dielectric measurements for corn leaves, it appears to provide a good fit to other types of vegetation as well. An example is shown in Fig. 4-45 for rubber leaves (Chuah et al., 1995).

PROBLEMS

4.1 Use Computer Code 4.1 to determine the microwave frequency at which the dielectric loss factor of pure water at 10 °C is a maximum in the range 1 to 30 GHz.

4.2 Use Computer Code 4.2 to generate plots for the relative permittivity and dielectric loss factor of saline water, at $T = 20$ °C and $f = 3$ GHz, as a function of salinity over the range from 0 to 40 psu.

4.3 Use Computer Code 4.3 to generate a plot of the dielectric loss factor of pure ice at 1 GHz as a function of temperature over the range from -1 °C to -30 °C.

4.4 For pure ice at $T = -20$ °C, below what frequency is the penetration depth greater than:

(a) 1 m?

(b) 10 m?

(c) 100 m?

4.5 Randomly oriented ice inclusions with

$$\varepsilon_i = 3.2 - j0.02$$

are present in an air background. Compute and plot the equivalent TVB permittivity and dielectric loss factor of the mixture as a function of the inclusion volume fraction, assuming the inclusions to be:

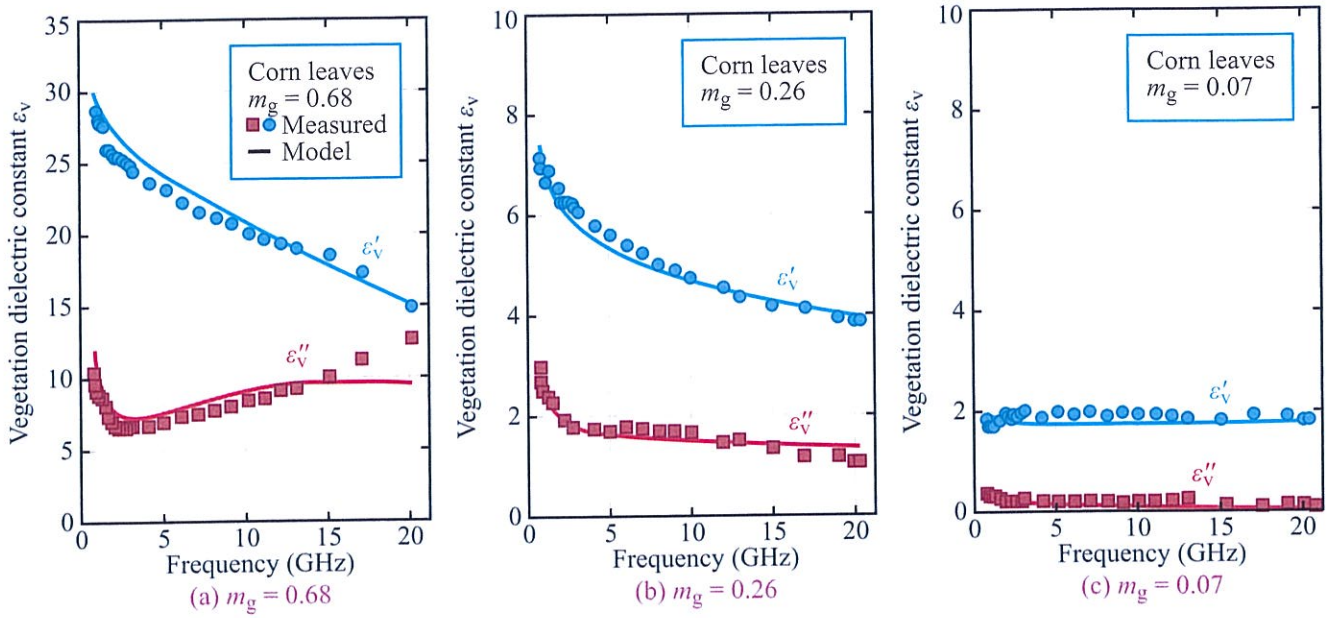

Figure 4-43: Comparison of the dielectric spectrum predicted by the vegetation model with measured data at (a) $m_g = 0.68$, (b) $m_g = 0.26$, and (c) $m_g = 0.07$.

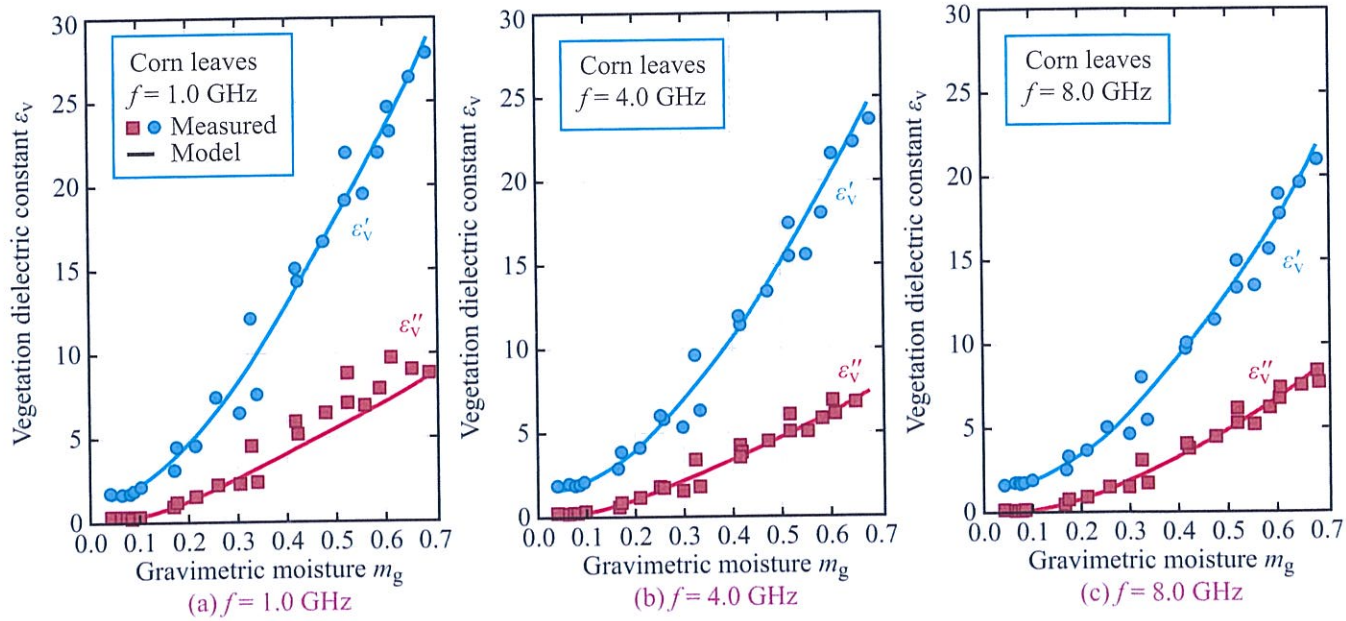

Figure 4-44: Comparison of the dielectric variation with moisture as predicted by the vegetation model with data at (a) 1 GHz, (b) 4 GHz, and (c) 8 GHz.

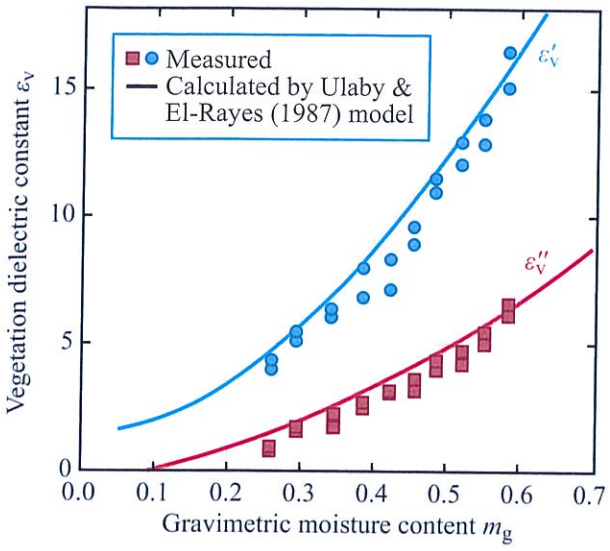

Figure 4-45: Dielectric constant of rubber leaves at 10.0 GHz [Chuah et al., 1995].

(a) circular discs,

(b) spheres,

(c) needles.

Suggestion: Use Computer Code 4.4.

4.6 A certain medium is modeled as a mixture of randomly oriented ellipsoids in a background of air. The ellipsoid dimensions are $2a_1 = 2b_1 = 0.12$ mm and $2c_1 = 1.76$ mm, and the dielectric constant of the ellipsoid material is $\varepsilon_i = 3.2 - j0.1$. Use the TVB model to develop an expression for the dielectric constant of the mixture, and then plot it as a function of the inclusion volume fraction.

4.7 Use the refractive model given by Eq. (4.45) with $\alpha = 1/2$ to compute the real and imaginary parts of the dielectric constant of a mixture composed of ice with $\varepsilon_i = 3.2 - j0.02$ in an air background. Plot your results as a function of the inclusion volume fraction.

4.8 Based on the data in Fig. 4-4, we estimate ε''_i of slightly impure ice at $T = -1$ °C and $f = 8.6$ GHz to be $\approx 4 \times 10^{-3}$. Use this value to compute the loss factor of dry snow and then to compute:

(a) ε''_{ds} as a function of ice volume fraction v_i.

(b) the penetration depth as a function of v_i.

4.9 Use Computer Code 4.6 to compute and plot the penetration depth in wet snow as a function of snow wetness (from 0 to 12%). The snow density is 0.4 g/cm^3 and the frequency is 10 GHz.

4.10 Use Computer Code 4.7 to compute and plot the penetration depth in wet soil as a function of volumetric soil moisture (from 3% to 30%) at 1.4 GHz. Assume $T = 20$ °C, the sand fraction $S = 30\%$, and the clay fraction $C = 50\%$.

4.11 Use Computer Code 4.8 to generate a Cole-Cole plot [similar to that in Fig. 4-42(b)] for vegetation with a gravimetric moisture content of 0.5. Assume the salinity of the vegetation fluid to be 7 psu.